ELSEVIER

Coordination Chemistry Reviews 230 (2002) 193–211

COORDINATION CHEMISTRY REVIEWS

www.elsevier.com/locate/ccr

Ligand-to-ligand charge transfer states and photochemical bond homolysis in metal–carbon bonded platinum complexes

Joris van Slageren [a,*], Axel Klein [b,*], Stanislav Záliš [c,*]

[a] *Institute of Molecular Chemistry, Universiteit van Amsterdam, Nieuwe Achtergracht 166, NL-1018 WV Amsterdam, The Netherlands*
[b] *Institut für Anorganische Chemie, Universität Stuttgart, Pfaffenwaldring 55, D-70569 Stuttgart, Germany*
[c] *J. Heyrovský Institute of Physical Chemistry, Academy of Sciences of the Czech Republic, Dolejškova 3, CZ-18 000 Prague 8, Czech Republic*

Received 19 September 2001; accepted 8 March 2002

Contents

Abstract

This paper reviews the photochemical Pt–C bond homolysis reactions of metal–carbon bonded platinum compounds. Three types of complexes are considered: [Pt(R)$_2$(COD)], [Pt(R)$_2$(α-diimine)] and [Pt(Me)$_4$(α-diimine)]. This photoreactivity originates in the involvement of the σ-bonded co-ligands in low-lying excited states. This involvement was proved by time-dependent density-functional theory (TD DFT) calculations and resonance Raman (rR) spectroscopy. In the case of the platinum(II) complexes, the contribution of the co-ligand to the high-lying filled orbitals increases with increased σ-donor strength of this ligand. Concurrently, the photoreactivity increases dramatically in the case of the [Pt(R)$_2$(COD)] complexes. The corresponding α-diimine analogues are much less reactive due to the smaller co-ligand participation in high-lying filled orbitals. The platinum(IV) complexes [Pt(Me)$_4$(α-diimine)] are very photoreactive, due to the fact that the HOMO has almost exclusively σ(C_{ax}–Pt–C_{ax}) character.

Keywords: Platinum complexes; Ligand-to-ligand charge transfer states; Sigma-bond-to-ligand charge transfer states; Resonance Raman spectroscopy; Photochemistry; DFT calculations

* Corresponding authors.
E-mail addresses: slageren@anorg.chem.uva.nl (J. van Slageren), aklein@iac.uni-stuttgart.de (A. Klein), zalis@jh-inst.cas.cz (S. Záliš).

0010-8545/02/$ - see front matter
PII: S0010-8545(02)00092-9

1. Introduction

In the majority of complexes formed by low-valent transition metal atoms and ligands with low-lying empty orbitals, in particular α-diimines, the lowest excited state is of the metal-to-ligand charge transfer (MLCT) type. Indeed, a great deal of today's research into subjects ranging from electron and energy transfer to light harvesting complexes and light-driven molecular machines revolves around such MLCT states [1–4]. In most of these complexes, the co-ligands, if present, are not involved in any low-lying electronic transitions. However, co-ligands with relatively high lying filled orbitals may participate in the orbital from which low lying electronic transitions originate (highest occupied molecular orbital (HOMO)). This can change the photophysical and photochemical properties of the resulting complexes dramatically. For example, the fact that the HOMO of the famous N3 dye molecule (N3 = *cis*-$[Ru(NCS)_2(dcbH_2)_2]$, $dcbH_2$ = 4,4′-dicarboxy-2,2′-bipyridine) is partly located on the NCS^- ligands facilitates the reduction of its oxidized form and may thus be a key to its success in dye-sensitized solar cells [2].

The study of photophysical and photochemical properties of complexes and clusters in which the co-ligands perform a major role in the excited state properties have been one of the main research interests of Professor Stufkens, to whom this issue is dedicated. One example of co-ligands with high lying filled orbitals are formed by the heavier halide atoms. Octahedral d^6 configured complexes of late transition metals like $[Ru(Cl)(Me)(CO)_2(\alpha\text{-diimine})]$ and $[Re(Cl)(CO)_3(\alpha\text{-diimine})]$ have virtually pure lowest MLCT transitions and excited states. The character of the lowest-energy electronic transition was confirmed by resonance Raman (rR) spectroscopy [5,6]. The merit of this technique is based on the fact that the Raman intensities of those vibrations are strongly enhanced, which are coupled to the electronic transition which belongs to the absorption band into which irradiation occurs. Conversely, by recording the rR spectrum, information is obtained about the electronic transition, which is excited [7]. Recent CASSCF/CASPT2 MO calculations confirmed the prevailing MLCT character of the lowest electronic transition of $[Ru(Cl)(Me)(CO)_2(Me\text{–}DAB)]$ (Me–DAB is *N*,*N*′-dimethyl-1,4-diazabutadiene) [8]. However, in the corresponding iodide complexes, the lowest transition originates almost exclusively from the halide atom, due to its higher p-orbital energy, with respect to chloride. Once again this assignment was supported by rR spectra [5,6]. Hence the lowest electronic transition has ligand-to-ligand charge transfer (L′LCT) character, which in this case of halide atoms has also been called halide-to-ligand charge transfer (XLCT). This change in electronic transition type has some consequences for the excited state properties. Time resolved IR measurements showed that the change in ν(CO) in the excited state and thus the amount of charge that has been transferred from the central metal atom to the α-diimine ligand decreases going from X = Cl to I in $[Ru(X)(Me)(CO)_2(^i Pr\text{–}DAB]$. As a result of this decreased charge transfer character, the iodide complex is less distorted in the excited state, which slows down non-radiative decay and hence increases the lifetime from 0.3 to 1.8 μs going from X = Cl to I [9].

In some cases an L′LCT state can only be populated indirectly. The lowest-energy excited state of several Re(I)-based chromophore-quencher (C–Q) complexes has L′LCT character [10–12]. Since the electronic interaction between donor and acceptor is weak, the optical L′LCT transition of these C–Q complexes has an extremely low extinction coefficient (e.g. $\varepsilon = 2.4\ M^{-1}\ cm^{-1}$ in the case of $[Re(py\text{-}PTZ)(CO)_3(bpy)]^+$; py-PTZ = phenothiazine-functionalised pyridine). However, the L′LCT state can be populated indirectly, by optical $d_\pi(Re) \rightarrow \pi^*(bpy)$ MLCT excitation followed by py-PTZ → Re intramolecular electron transfer. The decay to the ground state is mainly non-radiative and the excited state properties must be studied by transient absorption spectroscopy, or indirectly by the effect on the MLCT excited state lifetime of the chromophore. If the donor ligand is sensitive to oxidation, photochemical ligand fragmentation may occur [13].

A very interesting situation is that in which the orbital from which the electron density originates is the one that binds metal and co-ligand together. The special type of L′LCT state that results from charge transfer from this σ orbital to the π accepting ligand has been named a sigma-bond-to-ligand charge transfer (SBLCT) [14] or σπ* [15] state.

In the Amsterdam laboratory many complexes possessing such SBLCT states have been investigated. In some cases, the SBLCT state is not optically accessible, e.g. $[Re(L)(CO)_3(\alpha\text{-diimine})]$. For L = Me, the SBLCT state is higher in energy than the MLCT one. The fact that the photochemical quantum yield for e.g. $[Re(Me)(CO)_3(dmb)]$ (dmb = 4,4′-dimethyl-2,2′-bipyridine) is appreciable ($\Phi = 0.42$ in toluene at 293 K) [16] was indeed found to be due to prompt chemical reaction from the Franck–Condon state, rather than reaction from the lowest excited state [17]. On increasing the σ donor strength of the σ bound axial ligand, the corresponding σ(Re–L) bond rises in energy. As a consequence the lowest excited state obtains SBLCT character. This leads to the efficiency of photochemical bond homolysis approaching unity in the case of R = Et, *iso*-propyl (^{i}Pr) in the complexes $[Re(R)(CO)_3(dmb)]$ [16]. The difference is even larger upon replacement of the dmb ligand by ^{i}Pr–DAB, which results in a drastic decrease of the photoreactivity to a few percent for R = Me, while the efficiency remains over 0.7 for R = Et or Bzl [18]. The enhancement of photochemical reactivity

by increasing the σ donor strength of the ligand is a recurring theme in this review and indeed in the photochemistry of metal–alkyl complexes. Thus, whereas the complexes [Ru(I)(R)(CO)$_2$(^{i}Pr–DAB)] (R = Me, Et) are photostable, the corresponding ^{i}Pr complex gives rise to efficient photoinduced Ru–C bond homolysis [19]. Recently the observed photochemical radical formation in the complexes *cis*-[Rh(R)$_2$(I)(CO)(dmb)] (R = Me, ^{i}Pr; dmb = 4,4′-dimethyl-2,2′-bipyridine) was proposed to occur via such an SBLCT state [20]. In other cases the SBLCT states are directly optically accessible, e.g. in [M(L$_1$)(L$_2$)(CO)$_2$(α-diimine)] (M = Ru, Os, L$_1$, L$_2$ = alkyl group or metal fragment). In these complexes photochemical bond homolysis reactions quantum yields varying from a fraction of a percent [21] to very efficient [22] were observed. Whenever the photochemical reaction is retarded, e.g. in case the bond from the central metal atom is strong or under certain conditions, such as low temperatures, these complexes can have exceedingly long excited state lifetimes of up to 1 ms [21,23–25].

Some L′LCT and SBLCT transitions and excited states have been identified in platinum chemistry. Recently is has been shown, that the d^6 platinum(IV) complexes [PtMe$_4$(α-diimine)] have a lowest SBLCT transition and excited states [26–28]. The photochemical properties of these complexes will be described in detail below. In the case of platinum(II) complexes L′LCT transitions have been found for platinum α-diimine bisthiolate complexes [29–33]. Here, mainly the sulfur p orbitals form the HOMO and the resulting lowest transition is assigned to a L′LCT [29,32,34]. Since the interaction is mediated by the metal or admixed with metal orbitals it is also referred to as 'mixed metal-ligand-to-ligand' charge transfer (MML′LCT) [35].

This paper aims at reviewing the electronic structure, the spectroscopy and the photochemistry of platinum–carbon bonded complexes. Hence aforementioned Pt–S complexes are outside of the scope of this paper. Three types of complexes will be dealt with (Fig. 1). Firstly, the [Pt(R)$_2$(COD)] complexes, where increasing electron donating capabilities of the alkyl ligands causes their greater involvement in low-lying excited states. Secondly, replacing the COD ligand with its rather high lying π* orbital by the α-diimine ligand ^{i}Pr–DAB (^{i}Pr–DAB = *N*,*N*′-diisopropyl-1,4-diazabutadiene), shifts the lowest-energy absorption bands of the resulting complexes [Pt(R)$_2$(^{i}Pr–DAB)] into the visible region. The final example are the platinum(IV) diimine complexes [Pt(Me)$_4$(diimine)], which have a lowest-energy SBLCT transition and excited state. The assignments of the low-energy electronic transitions are based on density-functional theory (DFT) calculations and rR measurements. Furthermore the photochemical properties of the resulting complexes will be discussed. In this review, the emission properties of the excited states will not be considered. Among the luminescent platinum carbon bonded compounds are the [Pt(R)$_2$(α-diimine)] complexes with R = cyanide, mesityl, or acetylide [36–43].

2. Experimental

2.1. General

Syntheses, characterizations and measurements have been performed according to published procedures [26,28,44–46].

2.2. Theoretical calculations

Ground state electronic structure calculations on the complexes have been done on the base of DFT methods using the ADF2000.2 [47,48] and GAUSSIAN 98 [49] program packages. The lowest excited states of the closed shell complexes were calculated by the time-dependent DFT (TD DFT) method (both ADF and G98 programs). The electrostatic solvent effect was modeled by the polarizable continuum model, incorporated into GAUSSIAN 98 [50].

Within the ADF program, Slater type orbital (STO) basis sets of triple-ζ quality with polarization functions were employed, methyl groups on Mes ligands were described by basis sets of double-ζ quality with polarization functions. The inner shells were represented by frozen core approximation (1s for C, N, and 1s–4d for Pt were kept frozen). The following density functionals were used within ADF: the local density approximation (LDA) with VWN parameterization of electron gas data or the functional including Becke's gradient correction [51] to the local exchange expression in conjunction with Perdew's gradient correction [52] to the LDA expression (ADF/BP). The scalar relativistic (SR) zero order

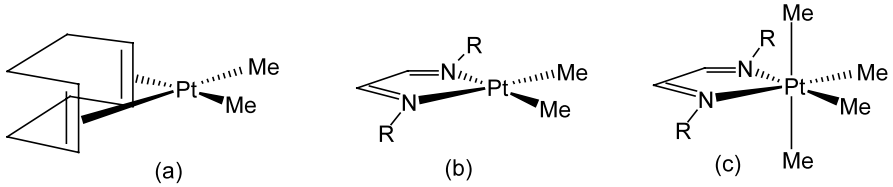

Fig. 1. Schematic structure of the complexes.

regular approximation (ZORA) [53] was used within this study. Within GAUSSIAN 98 Dunning's polarized valence double-ζ basis sets [54] were used for C, N and H atoms and the quasirelativistic effective core pseudopotentials and corresponding optimized set of basis functions [55] for Pt. Hybrid Becke's three parameter functional with Lee, Yang and Parr correlation functional (B3LYP) [56] was used in GAUSSIAN 98 calculations (G98/B3LYP). GAUSSIAN 98 was used for the calculations of the vibrations at G98/B3LYP optimized geometries.

The calculations on the complexes were performed in C_{2v} or constrained symmetry, respectively. The z axis is coincident with C_2 symmetry axis, the central atom and the α-diimine ligand lie in the yz plane. All results discussed correspond to optimized geometries.

3. Metal–carbon bonded platinum(II) complexes

3.1. Introduction

In Section 2, the electronic structure and photochemistry of two types of platinum(II) complexes are discussed, namely the complexes $[Pt(R)_2(COD)]$ and the $[Pt(R)_2(\alpha\text{-diimine})]$ compounds. The remainder of this introductory section gives a brief overview of what is known about the photochemistry of metal–carbon bonded platinum(II) complexes [57]. Platinum(II) metallacyclopentane complexes bearing phosphine ligands have been reported by Puddephatt to show photochemically induced decomposition reactions that can mainly be classified as reductive eliminations [58]. Similar reactivity was reported for diethyl platinum(II) complexes with phosphine ligands [59]. The corresponding methyl complexes gave CH_4 as the main product in C_6D_6 solution implying a α-hydride abstraction. In chlorinated solvents the monochloro complexes were found. Upon irradiation of neopentyl or neosilyl platinum complexes with phosphine ligands, Lappert was able to detect spin-trapped alkyl radicals by EPR [60]. Müller and Göser reported that the platinum(0) complex $[Pt(COD)_2]$ can be synthesized by photoinduced reductive elimination of the ^{i}Pr groups of $[Pt(^iPr)_2(COD)]$ [61]. Furthermore some aspects of the *cis–trans* photoisomerization of $[Pt(Ph)Cl(PEt_3)_2]$ were investigated, but also here, no definite assignment could be given [62]. One other example of photochemistry of metal–carbon bonded platinum(II) complexes, is the photoinitiated oxidative addition of organometallic platinum(II) complexes. For oxidative addition reactions with square planar d^8 platinum(II) complexes three mechanisms are known. First of all, there is the S_N2 type of reaction, in which the metal as a nucleophile substitutes one part of the substrate, followed by addition of the leaving group. Then, the oxidative addition can occur in a concerted one-step reaction. The last type mechanism involves a radical formed from e.g. an alkyl halide, which reacts with the platinum(II) species, forming a five coordinated Pt complex. This species proceeds to abstract a halide atom from another alkyl halide molecule, resulting in the oxidative addition product and another organic radical. As a non-chain reaction alternative to this last mechanism, the platinum(II) starting compound can form a charge transfer salt with the alkyl, followed by formation of a covalent bond with the halide and finally with the organic radical [63,64]. The radical chain mechanism was found to operate in the reaction of ^{i}PrI with $[Pt(Me)_2(phen)]$ [63]. Thus, the triplet excited state of $[Pt(Me)_2(phen)]$ abstracts a iodide from the alkyl halide, yielding an ^{i}Pr$^\bullet$ radical, which in turn reacts with the starting compound and consequently with another molecule of ^{i}PrI to yield the oxidative addition product and another ^{i}Pr$^\bullet$ radical. Another photoinduced oxidative addition occurs in the reaction of MeI to$[Pt(CH_3)_2(COD)]$ leading to the tetramer $[Pt(I)(Me)_3(COD)]_4$ with a quantum yield of $\Phi = 0.005$ at $\lambda_{irr} = 313$ nm [65].

This last reaction was proposed to occur from a $\sigma CH_3^- \rightarrow \pi^*(COD)$ L′LCT excited state. In order to increase the photoreactivity of such complexes, more electron donating alkyl substituents were introduced. The results are described in the following section.

3.2. $[Pt(R)_2(COD)]$ complexes

The COD ligand is well known to stabilize very electron rich late transition metal fragments. It has a non conjugated π system and, therefore, the lowest empty orbitals are rather high in energy. As a result the lowest-energy absorption bands are located in the near-UV region of the spectrum and the complexes are off-white in color. Following the preliminary investigation of the photoreactions of $[Pt(CH_3)_2(COD)]$ by Vogler [65], we prepared a series of $[Pt(R)_2(COD)]$ complexes to investigate the electronic structure, the electronic transitions and the photochemistry of electron rich COD platinum(II) complexes thoroughly [44]. In part of this series the σ-donor strength of the R ligand is increased, going from R=methyl (CH_3) to trimethylsilylmethyl (neosilyl, neoSi) to benzyl (Bzl) to 2-methyl-2-phenyl-1-propyl (neophyl = neoPh) to 2,2-dimethyl-1-propyl (neopentyl, neop) to 1-adamantylmethyl (adme), and finally to ^{i}Pr. Furthermore alkynyl (C≡CPh, C≡C^{t}Bu). In the following, first the character of the various molecular orbitals and the influence of the R group thereon is discussed.

3.2.1. Molecular orbital structure

Whereas the lowest π* orbital of COD is expected to be the lowest unoccupied molecular orbital (LUMO), the character of the HOMO is more ambiguous. In

general the HOMO in d^8 square planar platinum(II) complexes has been thought to be one of the filled metal d orbitals. Thus, in the complexes *cis*- and *trans*-$[Pt(L_1)(L_2)(PEt_3)_2]$ (L_1, L_2 = Me, Et, Cl, Br) most low lying transitions were assigned to metal-to-ligand (phosphine) charge transfer transitions. Only in the case of the halide complexes additional ligand-to-metal charge transfer (LMCT) and ligand field (LF) transitions were observed [66]. The former type of transition occurs from the halide to the metal in these complexes at relatively low energy, due to the presence of high lying filled p orbitals on the halides. The latter can occur, due to the low LF strength of the halides. However, in the case of $[Pt(Me)_2(COD)]$ the HOMO was proposed to have σCH_3^- character [65], based on the observed photolability and some early MO calculations. These self-consistent-field-Xα-scattered-wave (SCF-Xα-SW) calculations described the HOMO in $[Pt(Me)_2(PH_3)_2]$ as Pt–C bonding.

In order to clear up the problem of the assignment of the frontier orbitals of the $[Pt(R)_2(COD)]$ complexes, DFT MO-calculations were performed on several complexes. Apart from the MO scheme of the parent compound, $[Pt(Me)_2(COD)]$, also that of $[Pt(^iPr)_2(COD)]$ was calculated. The latter compound possesses the stronger σ donating ligand ^{i}Pr, which can be expected to result in a greater participation of the alkyl orbitals in the HOMO of the complex. As an example of a complex with unsaturated σ-bound ligands the $[Pt(C{\equiv}CH)_2(COD)]$ model complex was included. The compositions of the highest filled and lowest unfilled orbitals of $[Pt(Me)_2(COD)]$ are shown in Table 1, while Figs. 2 and 3 show contour plots of the HOMO and LUMO, respectively. From Table 1 and Fig. 2 it is clear that the HOMO ($16a_1$) mainly consists of the bonding combination of a variety of metal orbitals together with the sp^3 like methyl orbitals and has a small π(COD) contribution. Indeed the first virtually pure metal orbital ($15a_1$) is located 0.87 eV (7000 cm^{-1}) below the HOMO. Below that lies an orbital, which has mixed π(COD) and methyl character. The remaining

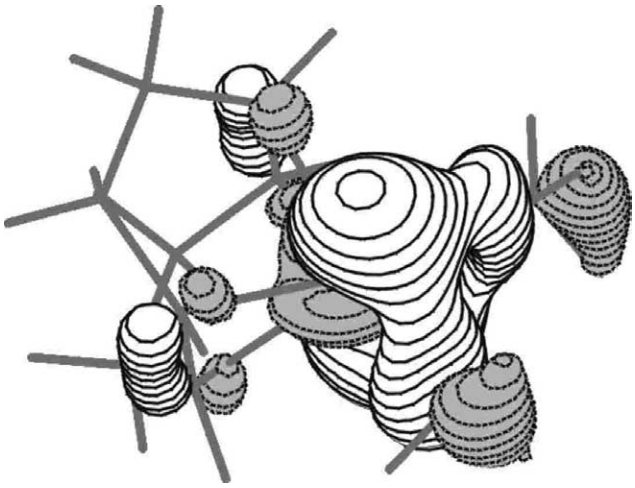

Fig. 2. $16a_1$ HOMO $[Pt(Me)_2(COD)]$.

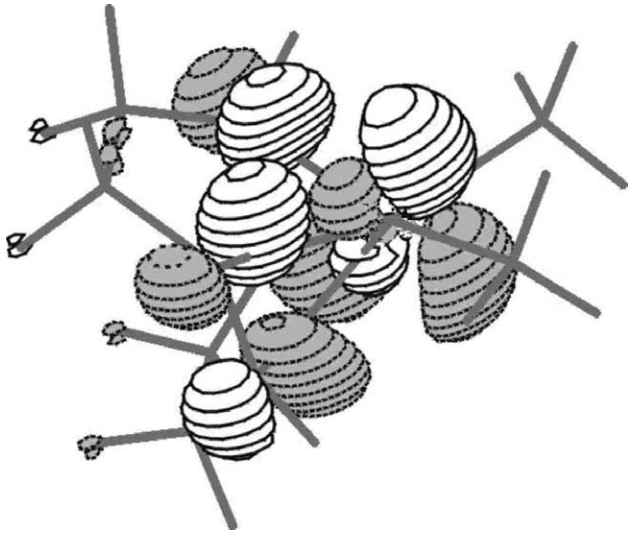

Fig. 3. $11b_1$ LUMO $[Pt(Me)_2(COD)]$.

Table 1
DFT calculated one-electron energies and percentage composition of selected HOMO and LUMO of $[Pt(Me)_2(COD)]$ expressed in terms of composing fragments

MO	*E* (eV)	Prevailing character	Pt	Me	COD
Unoccupied					
$13b_2$	−0.21	d_{Pt}+Me+COD	2 (p_y); 29 (d_{yz})	48	23
$8a_2$	−0.71	π* COD	12 (d_{xy})		88
$11b_1$	−1.71	π* COD	11 (p_x); 13 (d_{xz})	4	72 (π*)
Occupied					
$16a_1$	−5.01	d_{Pt}+Me+COD	15 (s); 2 (p_z); 34 ($d_{x^2-y^2}$); 6 (d_{z^2})	31	12 (π)
$15a_1$	−5.88	d_{Pt}	1 (s); 70 (d_{z^2}); 3 ($d_{x^2-y^2}$)	13	6
$12b_2$	−6.01	π_{COD}+Me	5 (p_y); 4 (d_{yz})	34	56
$7a_2$	−6.19	d_{Pt}	72 (d_{xy})	11	16
$14a_1$	−6.28	d_{Pt}+Me+COD	4 (p_z); 38 ($d_{x^2-y^2}$); 3 (d_{z^2})	20	34
$10b_1$	−6.29	d_{Pt}	1 (p); 69 (d_{xz})	9	20

Table 2
DFT calculated one-electron energies and percentage composition of selected HOMO and LUMO of [Pt(^{i}Pr)$_2$(COD)] expressed in terms of composing fragments

MO	E (eV)	Prevailing character	Pt	^{i}Pr	COD
Unoccupied					
$14b_1$	−1.91	π*(COD)	12 (p_x); 16 (d_{xz})	5	67 (π*)
Occupied					
$19a_1$	−4.82	$d_{Pt}+{}^i$Pr+π(COD)	18 (s); 2 (p_z); 24 ($d_{x^2-y^2}$); 5 (d_{z^2})	43	7 (π)
$15b_2$	−5.81	π(COD)+^{i}Pr+Me	10 (p_y); 4 (d_{yz})	41	44
$18a_1$	−5.92	d_{Pt}	1 (s); 75 (d_{xy})	16	8
$10a_2$	−6.21	d_{Pt}	78 (d_{xy})	13	8

orbitals in the shown energy interval have highly mixed metal–methyl-COD character. In the region of the unoccupied MOs, the LUMO has predominant π*(COD) character, as does the orbital above it. The LUMO+2 has a mixed metal–methyl-COD composition. Since the HOMO of [Pt(Me)$_2$(COD)] is the bonding combination of metal and methyl orbitals, the introduction of more σ donating alkyl groups can be expected to lead to even larger involvement of the alkyl group in the HOMO, which in turn could lead to increased photoreactivity. Indeed Table 2 shows that the $19a_1$ HOMO of [Pt(^{i}Pr)$_2$(COD)] has an alkyl group contribution of 43% compared with only 31% for the methyl derivative. Concurrent with the higher involvement of the alkyl group, the HOMO has risen in energy from −5.01 to −4.82 eV going from the methyl to the ^{i}Pr complex. The Pt contribution to the HOMO has decreased by more or less the same amount as the increase of the ^{i}Pr contribution. The LUMO character of [Pt(^{i}Pr)$_2$(COD)] is virtually unchanged with respect to the methyl complex.

In the case that the σ bonded ligand has filled π orbitals, the MOs obtain a slightly different character. This can be seen from Table 3, which reports the results of the DFT calculated MOs of [Pt(C≡CH)$_2$(COD)], which can be viewed as a model complex for [Pt(C≡CPh)$_2$(COD)] and [Pt(C≡C^{t}Bu)$_2$(COD)]. From Table 3 it is clear that the close spaced four highest filled orbitals are mainly π(C≡CH) in character and that the maximum metal contribution in this set of orbitals is 20% (in the $17a_1$ HOMO). Only the $16a_1$ HOMO-4, at 0.7 eV (5600 cm^{-1}) below the HOMO has predominant metal character (79%). Similar results were obtained for [Pt(Ph)$_2$(COD)] [44].

3.2.2. Spectroscopy and electronic transitions

As noted before, the complexes [Pt(R)$_2$(COD)] absorb only in the ultraviolet. The maximum of the lowest absorption band of the alkyl substituted [Pt(R)$_2$(COD)] complexes varies between 358 nm for R = Me and 395 nm for R = ^{i}Pr (a difference of 2600 cm^{-1}) [44]. They follow almost perfectly the order of σ donating abilities of the alkyl ligand. The extinction coefficients are all quite low, around 150 M^{-1} cm^{-1}. Furthermore around 285 and 250 nm, there are two more absorption bands with extinction coefficients of ∼1000–1500 and ∼2500–3500 M^{-1} cm^{-1}, respectively. In the case of R = neoPh, Bzl, these transitions are obscured by the much more intense ππ* transitions of the phenyl rings. The alkynyl complexes have four absorption bands above 250 nm as well. However, in view of their different orbital character, they probably belong to slightly different types of transitions. All absorption

Table 3
DFT calculated one-electron energies and percentage composition of selected HOMO and LUMO of [Pt(C≡CH)$_2$(COD)] expressed in terms of composing fragments

MO	E (eV)	Prevailing character	Pt	CCH	COD
Unoccupied					
$14b_2$	−1.21	d_{Pt}+CCH+COD	5 (p_y); 33 (d_{yz})	40	22
$8a_2$	−1.37	π* COD	9 (d_{xy})	9	89
$11b_1$	−2.52	π* COD	16 (p_x); 8 (d_{xz})	8	59 (π*)
Occupied					
$17a_1$	−5.51	π CCH+d_{Pt}	1 (s); 11 ($d_{x^2-y^2}$); 8 (d_{z^2})	77	3 (π)
$7a_2$	−5.64	π CCH	11 (d_{xy})	86	3
$13b_2$	−5.69	π CCH	–	96	4
$10b_1$	−5.94	π CCH+d_{Pt}	2 (p_x); 10 (d_{xz})	78	10
$16a_1$	−6.21	d_{Pt}	10 (s); 1(p_z); 38 ($d_{x^2-y^2}$); 30 (d_{z^2})	13	6

Table 4
TD DFT calculated lowest singlet excitation energies (eV and nm), oscillator strengths and observed absorption maxima for $[Pt(Me)_2(COD)]$ [a]

State	Composition	Transition energy in eV (nm)	Oscillator strength	Absorption maxima found (ε) [b]	Absorption maxima found (ε) [c]
$^1B_1$	98% ($16a_1 \rightarrow 11b_1$)	3.61 (343)	0.002	358 (140)	352 (150)
$^1B_1$	98% ($15a_1 \rightarrow 11b_1$)	4.36 (284)	0.001	318 (700)	318 (790)
$^1B_1$	91% ($14a_1 \rightarrow 11b_1$)	4.78 (260)	0.022	290 (1400)	286 (1340)
$^1B_2$	82% ($7a_2 \rightarrow 11b_1$); 14% ($16a_1 \rightarrow 13b_2$)	4.87 (254)	0.007	258 (110)	262 (170)
$^1A_1$	74% ($10b_1 \rightarrow 11b_1$);10% ($7a_2 \rightarrow 8a_2$)	5.12 (242)	0.042	248 (2600)	248 (2350)
$^1A_1$	92% ($16a_1 \rightarrow 17a_1$)	5.23 (237)	0.005	242 (120)	237 (200)
$^1B_1$	82% ($12b_2 \rightarrow 8a_2$)	5.78 (214)	0.033	n.d.[d]	218 (13 000)
$^1A_1$	99% ($16a_1 \rightarrow 18a_1$)	5.89 (210)	0.011	n.d.[d]	202 (19 250)

[a] Maxima (in nm) and extinction coefficients (in M^{-1} cm^{-1}) were extracted from spectral deconvolution.
[b] In CH_2Cl_2 solution.
[c] In MeCN solution.
[d] Not detected due to absorption of the solvent.

bands show slight negative solvatochromism, pointing to their charge transfer character.

In order to assign all absorption bands unambiguously, TD DFT calculations were performed on the $[Pt(R)_2(COD)]$ (R = Me, ^{i}Pr, C≡CH) complexes. The results are reported in Table 4 and Fig. 5. From Table 4 it can be seen that the three lowest-energy electronic transitions of $[Pt(Me)_2(COD)]$ are all overlap forbidden, which explains the low extinction coefficients. The lowest-energy absorption band is assigned to the spin-allowed HOMO→LUMO transition, which can be characterized as a σ(Pt–Me)→π*(COD) transition in agreement with the previous assignment. The lowest-energy electronic transition can thus be characterized as SBLCT. The corresponding excitation removes electron density from a bonding σ(Pt–Me) orbital which explains the observed photoreactivity. Due to the difference in medium (all calculations suppose vacuum as the medium) the calculated transition energies differ from the experimental ones by about 0.1–0.2 eV. The second absorption band ($15a_1 \rightarrow 11b_1$) has mostly MLCT character due to the predominant metal character of orbital $15a_1$. The third transition is calculated to have a stronger oscillator strength, which is reflected in a higher extinction coefficient. A weakly allowed transition is calculated at 254 nm, which is only extracted from the absorption spectrum by spectral deconvolution. Interestingly, this transition contains a contribution from the $16a_1$(HOMO)→$13b_2$(LUMO+2) transition. The first overlap allowed transition is calculated at 242 nm, and has mainly MLCT character. A number of higher transitions is calculated and assigned to absorption bands (Table 4). Within the calculated range no transitions between mainly platinum centered orbitals (LF transitions) are found. If they occur they must be higher in energy than 200 nm. Calculations on $[Pt(^iPr)_2(COD)]$ show that the electronic transitions in this complex have the same character as in the methyl derivative. However, the two lowest electronic transitions are bathochromically shifted, namely from 3.61 and 4.46 eV (R = Me) to 3.13 and 4.03 eV (R = ^{i}Pr), in accordance with the absorption spectrum.

Table 5 reports the calculated transition energies and characters for $[Pt(C{\equiv}CH)_2(COD)]$ as well as the absorption bands to which they are attributed. In this case the moderately strong absorption band (ε = 3240 M^{-1} cm^{-1}) has to be assigned to the spin allowed $7a_2 \rightarrow 11b_1$ (HOMO–LUMO) transition (L′LCT), in view of the calculated oscillator strengths. The ADF calculations resulted in transition energies that were much lower than the experimental ones. Calculations using GAUSSIAN 98 gave better agreement. Calculated transition energies are only moderately influenced by basis sets variations. The difference is due a Becke–Perdew versus B3LYP functional variation. For the same basis set quality the G98/BP calculations give similar transition energies as ADF/BP. This assignment of the HOMO–LUMO transition to the band at 307 nm, means that the absorption found at longer wavelengths (345 nm) should be the corresponding spin forbidden transition. Alternatively this absorption could be assigned to a 98% ($17a_1 \rightarrow 11b_1$) transition. From Gaussian calculations this transition is calculated at 3.51 eV (353 nm), with an oscillator strength of 0.0001 (Table 5).

The other strong absorption band belongs to an overlap allowed π(C≡CH)→π*(COD) transition ($10b_1 \rightarrow 11b_1$) (L′LCT) according to the present calculations. At 286 nm a band is found, that according to the calculations belongs to another transition with 98% $16a_1 \rightarrow 11b_1$ d(Pt)→π*(COD) (MLCT) character. Unfortunately, no direct experimental evidence could be obtained for the character of the lowest electronic transitions. The technique of choice to aid the assignment of visible absorption band to certain electronic

Table 5
TD DFT calculated lowest singlet excitation energies (eV or nm), oscillator strengths and observed absorption maxima [a] for $[Pt(C{\equiv}CH)_2(COD)]$

State	Composition	G98/B3LYP		ADF/BP		Absorption maxima found (ε) [a]
		Transition energy in eV (nm)	Oscillator strength	Transition energy in eV (nm)	Oscillator strength	
$^3B_2$ [b]	99% ($7a_2 \rightarrow 11b_1$)	3.24 (383)		2.98 (416)		345 (600)
$^1B_2$	96% ($7a_2 \rightarrow 11b_1$)	3.89 (310)	0.088	3.49 (355)	0.081	307 (3240)
$^1A_1$	88% ($10b_1 \rightarrow 11b_1$)	4.21 (294)	0.112	3.78 (328)	0.096	272 (3320)
$^1B_1$	98% ($16a_1 \rightarrow 11b_1$)	4.29 (289)	0.005	3.98 (310)	0.005	286 (720)

[a] Maxima (nm) and extinction coefficients ($M^{-1}\,cm^{-1}$) as observed for $[Pt(C{\equiv}C^tBu)_2(COD)]$ in CH_2Cl_2 solution.
[b] Alternative assignment $^1B_1$ [98% ($17a_1 \rightarrow 11b_1$)]; 3.51 eV (353); 0.0001 (G98/B3LYP calculated).

transitions, rR spectroscopy (see Section 1) could not be used, due to the fact that the available equipment is only suitable for visible light excitation

3.2.3. Photochemistry

Having established the participation of the σ-bonded ligands in the low lying excited states to a significant extent, the photochemical properties are discussed in this section. First of all, the photochemical product formation was studied by ^{1}H- and ^{13}C-NMR spectroscopic investigations of photolyzed oxygen-free CD_2Cl_2 solutions of the various compounds. For the photolysis in all cases a $\lambda > 320$ nm cut-off filter was used ensuring irradiation into the lowest-energy absorption band only. There proved to be three different types of photochemical reactions of these complexes, depending on the nature of the R group (Fig. 4). For the alkyl substituted complexes (except Me) photolysis under these conditions leads to the formation of the monochlorinated platinum complexes [Pt(Cl)(R)(COD)] (R = neoSi, neop, ^{i}Pr, adme, Bzl), the R–R coupling products and some chlorinated hydrocarbons. The NMR spectra of these products were compared with those of independently prepared samples. Prolonged irradiation of these monochlorinated complexes leads to the formation of $[Pt(Cl)_2(COD)]$ in high yields (60–80%). In the case of the dimethyl complex, the monochlorinated species is only formed in a minor amount. In this reaction the main product is the uncoordinated dimethylated 1,5-dimethylcyclooctane.

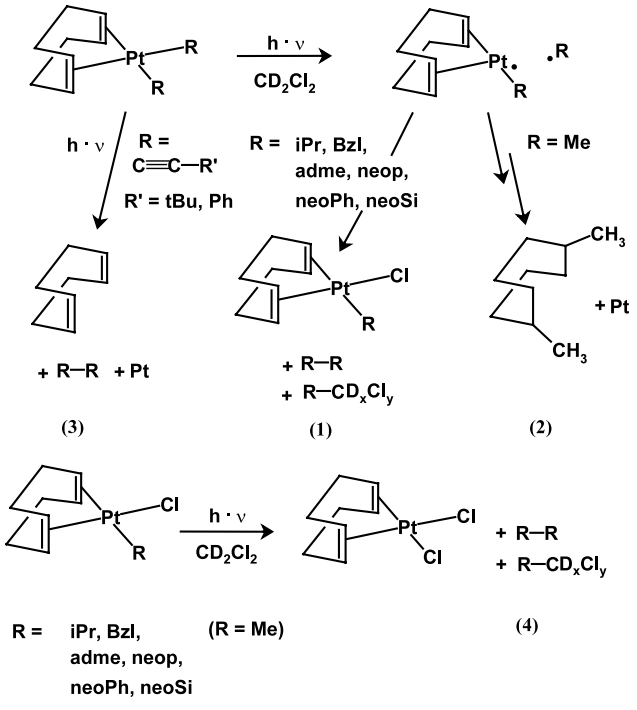

Fig. 4. Proposed reaction scheme for photochemical reactions of $[Pt(R)_2(COD)]$.

These reactions can be explained by the photochemical bond homolysis of the Pt–C bond. The organometallic radical proceeds to abstract a chlorine atom from the solvent. The organic radical can react with another organic radical or also abstract a chlorine atom from the solvent leading to the two observed organic photoproducts. The methyl radicals formed by photolysis of $[Pt(Me)_2(COD)]$ react with the unsaturated COD ligand within the solvent cage. Apparently they are more reactive than the other alkyl radicals. This type of ligand methylation is also found in photoreactions of $[Pt(Me)_4(R{-}DAB)]$ (see below) or $[Zn(R)_2(R{-}DAB)]$ [67]. In non-chlorinated solvents, the reactions following photochemical bond homolysis were found to lead to several non readily identifiable products. In contrast, irradiation of a hexane solution of $[Pt(^iPr)_2(COD)]$ in the presence of COD was reported to lead to the reductive elimination of the ^{i}Pr groups and the formation of $[Pt(COD)_2]$ [61]. The apparent incongruity can be explained along the following lines: the lowest electronic transition lowers the electron density in the σ(Pt–C) bonds to the same extent. This might give rise to both bond homolysis and reductive elimination. Apparently in chlorinated solvents the bond homolysis reaction is more efficient. Furthermore in the literature case, no cut off filter was used, which can lead to prompt reactions from higher lying excited states, the isolated yield being only 20%.

The alkynyl derivatives react in a slightly different way. The only products of their very clean photoreaction, that is independent of the solvent, are elemental platinum, COD and the R–R coupling product (Fig. 5). This reductive elimination was proposed to occur via a three membered ring (pericyclic) transition state, which involves the platinum atom and the two C_1 atoms of the alkynyl ligands [44]. The formation of such a transition state is facilitated by diminution of the electron density of the π system of the alkynyl ligands by the electronic transition. Similar reactions were found in the photoelimination of biaryls from bis(aryl)platinum(II) compounds [68]. The attribution of the observed photoreaction to this π mechanism pericyclic reaction [68] is supported by the observation that it is only observed for complexes with ligands that have π orbitals that are involved in the electronic transition. For these reactions the nature of the solvent was found not to be of influence.

Next, the relative rates of the photoreactions of $[Pt(R)_2(COD)]$ depending on the nature of R were studied. To this end, equimolar oxygen-free CD_2Cl_2 solutions of the compounds were irradiated, while the decay of the ^{1}H-NMR signals of the starting compound were followed as a function of time. Again a $\lambda > 320$ nm cut-off filter was used to ensure irradiation into the lowest absorption band only. This can cause an artifact in the found relative rates, since the absorption maxima of the complexes shift bathochromically with increasing σ donor strength of R. However, shorter wavelength irradiation ($\lambda > 295$ nm) of $[Pt(Me)_2(COD)]$ increased the photochemical reaction rate a mere 1.7 times, which is much less than the changes in rate as a function of R. Indeed, it was found that the relative rates increase along the series R = Me ($\equiv 1$) < neoSi (11) < neoPh (42) < neop (51) < ^{i}Pr (86) < adme (111) < Bzl (120). On the basis of purely inductive effects the order R = Me < neoSi < Bzl < neoPh < neop < adme < ^{i}Pr is expected. This means that both the Bzl and adme derivatives are more reactive than expected, and other factors must play a role. The observed increase in photoreactivity with increasing R donor strength is in excellent agreement with the MO calculations (see above). The alkynyl derivatives with R = C≡CPh or C≡C^{t}Bu were only slightly more reactive (relative rates 1.1 and 3.7, respectively) than the R = Me standard. However, the different type of photochemistry makes further comparison pointless.

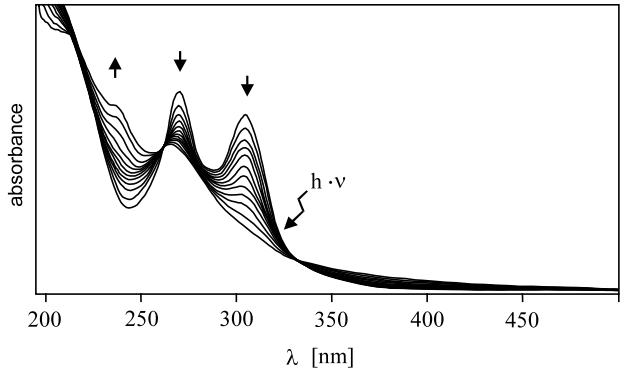

Fig. 5. Absorption spectra of $[Pt(C{\equiv}C^tBu)_2(COD)]$ in MeCN, during photolysis at $\lambda > 320$ nm. The traces are recorded with 20 s time intervals.

From the above it is clear, that on introduction of σ donating R substituents at the platinum(II) center, the photoreactivity of the resulting $[Pt(R)_2(COD)]$ complexes is enhanced dramatically. The use of alkynyl ligands leads to very clean photochemical formation of colloidal platinum(0) and the bis-alkynyl compound. However, all these photoreactions occur on near-UV irradiation due to the relatively high π* level of the COD ligand. Substitution of this ligand by one that has a lower lying empty orbital should shift the absorption bands into the visible region of the spectrum. This hypothesis is explored in the next section, by the introduction of α-diimine ligands.

3.3. $[Pt(R)_2(\alpha\text{-diimine})]$ complexes

Reports on photochemical reactivity of platinum(II)-α-diimine complexes are very sparse. The photoinitiated oxidative addition of ^{i}PrI to $[Pt(Me)_2(phen)]$ is one example (see Section 1) is one example [63]. Furthermore several platinum α-diimine dithiolate complexes were found to photooxidize in solution in the presence of molecular oxygen [69,70]. However, the results obtained for the $[Pt(R)_2(COD)]$ complexes described above suggested, that photochemical bond homolysis in the $[Pt(R)_2(\alpha\text{-diimine})]$ complexes should be possible. Therefore, we prepared several $[Pt(R)_2(R'-DAB)]$ (R′–DAB = *N*,*N*′-dialkyl-1,4-diazabutadiene) complexes, namely with R = CH_3, CD_3, neop, neoSi, adme, Ph, Mes, C≡C^{t}Bu, C≡CPh (for abbreviations, see previous section), in order to investigate their electronic structure and low lying electronic transitions as well as their photochemical reactivity. Their syntheses and structural and emission properties will be published elsewhere [46]. This section is organized similarly to the previous one.

3.3.1. Molecular orbital structure

The orbital energies and compositions of three (model) complexes were calculated using DFT methods. The influence of the σ donor capabilities of the σ bound ligands were investigated by calculations on $[Pt(Me)_2(^i Pr{-}DAB)]$ and $[Pt(^i Pr)_2(^i Pr{-}DAB)]$, the latter of which bearing the more σ-donating ^{i}Pr substituent. Unfortunately, this latter complex could not be isolated, but the observed trends are expected to be valid for other substituents that are more σ-donating than Me. Furthermore, the model complex $[Pt(C{\equiv}CH)_2(^i Pr{-}DAB)]$ was included, since the corresponding COD

Table 6
DFT calculated one-electron energies and percentage composition of selected HOMO and LUMO of [Pt(Me)$_2$(^{i}Pr–DAB)] expressed in terms of composing fragments

MO	E (eV)	Prevailing character	Pt	Me	^{i}Pr–DAB
Unoccupied					
16b$_2$	0.21	d_{Pt}+Me+^{i}Pr–DAB	2 (p_y); 35 (d_{yz})	48	15
9a$_2$	−0.30	π* ^{i}Pr–DAB	1 (d_{xy})		98
11b$_1$	−3.37	π* ^{i}Pr–DAB+d_{Pt}	18 (d_{xz}); 1 (p_x)	2	78 (π*)
Occupied					
19a$_1$	−4.77	d_{Pt}+Me	21 (s); 63 ($d_{x^2-y^2}$); 3 (d_{z^2})	12	
8a$_2$	−4.79	d_{Pt}	82 (d_{xy})	7	10
18a$_1$	−5.21	d_{Pt}+Me	4 (s); 72 (d_{z^2}); 5 ($d_{x^2-y^2}$)	12	4
10b$_1$	−5.43	d_{Pt}+π ^{i}Pr–DAB	68 (d_{xz}); 1 (p_x)	7	24
7a$_2$	−7.12	π ^{i}Pr–DAB	6 (d_{xy})	4	89

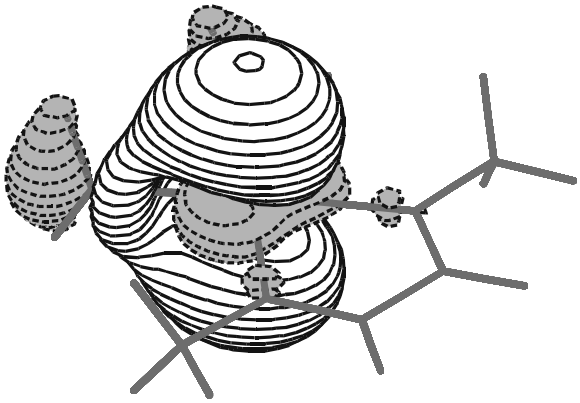

Fig. 6. 19a$_1$ HOMO [Pt(Me)$_2$(^{i}Pr–DAB)].

complex showed deviating photochemistry. The energies and percentage orbital compositions calculated for [Pt(Me)$_2$(^{i}Pr–DAB)] are reported in Table 6. It is clear from this Table that the 19a$_1$ HOMO is mainly Pt localized, with a small contribution of the sp^3(Me) orbitals (Fig. 6). The two orbitals below the HOMO (8a$_2$ and 18a$_1$) are similarly composed. Further down a mixed d(Pt)-π(^{i}Pr–DAB) orbital (10b$_1$) and a virtually pure π(^{i}Pr–DAB) orbital (7a$_2$) can be found. The first two unoccupied orbitals (11b$_1$ and 9a$_2$) are mainly composed of the ligand π* orbitals, like in the case of the COD complexes. On going from R = Me to ^{i}Pr (Tables 6 and 7) in the [Pt(R)$_2$(^{i}Pr–DAB)] complexes, as expected, the HOMO obtains more R group character (24 vs. 12%) and concurrently rises in energy (−4.27 vs. −4.77 eV, a difference of 4000 cm^{-1}). The LUMO (Fig. 7) remains unaffected by the change in R substituent as do the lower occupied orbitals. As expected the LUMO is much lower in energy for the [Pt(R)$_2$(^{i}Pr–DAB)] complexes (−3.37 and −3.34 eV in the case of R = Me and ^{i}Pr, respectively) than for the [Pt(R)$_2$(COD)] ones (−1.71 and −1.91 eV for R = Me and ^{i}Pr, respectively). The R-group contribution to the HOMO drops going from the COD complexes to the ^{i}Pr–DAB analogues, namely from 31 to 12% for R = Me and from 43 to 24% for R = ^{i}Pr. The reason might be that the rise in energy of the metal atoms decreases the overlap between metal and alkyl orbitals, decreasing the alkyl contribution to the high lying filled orbitals. The fact that there is no high-lying orbital with a predominant or even large methyl group contribution suggests that the photochemical reactivity of the [Pt(R)$_2$(α-diimine)] complexes should be diminished compared with the COD ones.

The electronic structure of [Pt(C≡CH)$_2$(^{i}Pr–DAB)] is somewhat different from that of the alkyl complexes. This is due to the fact that the alkynyl ligands have relatively high-lying filled π-orbitals. Thus the highest lying four MOs of the model complex have alkynyl

Table 7
DFT calculated one-electron energies and percentage composition of selected HOMO and LUMO of [Pt(^{i}Pr)$_2$(^{i}Pr–DAB)] expressed in terms of composing fragments

MO	E (eV)	Prevailing character	Pt	^{i}Pr	^{i}Pr–DAB
Unoccupied					
14b$_1$	−3.34	π* ^{i}Pr–DAB+d_{Pt}	16 (d_{xz}); 1 (p_x)	2	81 (π*)
Occupied					
22a$_1$	−4.27	d_{Pt}+^{i}Pr	24 (s); 44 ($d_{x^2-y^2}$); 8 (d_{z^2})	24	
11a$_2$	−4.60	d_{Pt}	85 (d_{xy})	6	7
21a$_1$	−5.16	d_{Pt}+^{i}Pr	2 (s); 67 ($d_{x^2-y^2}$); 10 (d_{z^2})	13	6
10b$_1$	−5.43	d_{Pt}+π ^{i}Pr–DAB	74 (d_{xz})	5	21
7a$_2$	−7.07	π ^{i}Pr–DAB	3 (d_{xy})	10	87

Table 8
ADF/BP calculated one-electron energies and percentage composition of selected HOMO and LUMO of [Pt(C≡CH)$_2$(^{i}Pr–DAB)] expressed in terms of composing fragments

MO	E (eV)	Prevailing character	Pt	C≡CH	^{i}Pr–DAB
Unoccupied					
$17b_2$	−0.68	d_{Pt}+CCH+^{i}Pr–DAB	8 (p_y); 38 (d_{yz})	30	23
$9a_2$	−0.65	π* ^{i}Pr–DAB	1 (d_{xy})		98
$11b_1$	−3.91	π* ^{i}Pr–DAB+d_{Pt}	12 (d_{xz})	10	78 (π*)
Occupied					
$8a_2$	−5.08	CCH+d_{Pt}	32 (d_{xy})	65	3
$20a_1$	−5.18	CCH+d_{Pt}	15 (d_{z^2}); 10 ($d_{x^2-y^2}$)	74	2
$10b_1$	−5.58	CCH+d_{Pt}+^{i}Pr–DAB	20 (d_{xz}); 2 (p_x)	62	16
$16b_2$	−5.62	CCH		98	2
$19a_1$	−5.79	d_{Pt}	21 (s); 52 ($d_{x^2-y^2}$); 23 (d_z2)	3	2
$7a_2$	−7.35	d_{Pt}+CCH+^{i}Pr–DAB	35 (d_{xy})	34	31

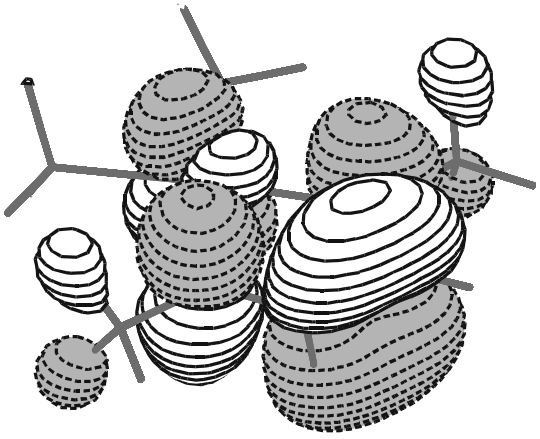

Fig. 7. $11b_1$ LUMO [Pt(Me)$_2$(^{i}Pr–DAB)].

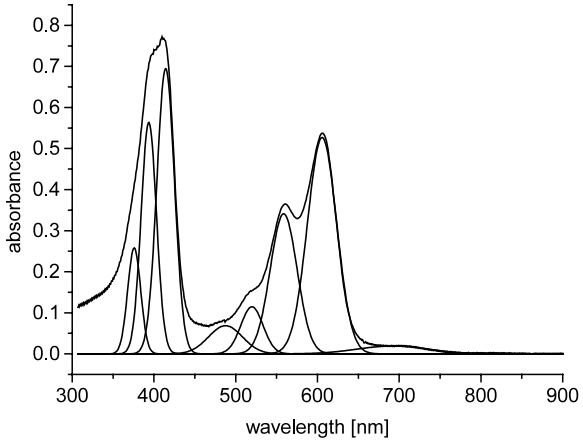

Fig. 8. Absorption spectrum of [Pt(Me)$_2$(^{i}Pr–DAB)] in pentane at room temperature, including spectral deconvolution of the absorption bands.

contributions of over 60% (Table 8). The platinum atom is involved in the $8a_2$ HOMO, the $20a_1$ HOMO-1, and the $10b_1$ HOMO-2, but the $16b_2$ HOMO-3 is of virtually pure alkynyl character. Recent IEH calculations (IEH, Iterative Extended Hückel) on [Pt(C≡CR)$_2$(phen)] (R = H, F, or Ph) show lower contributions (around 20%) of the alkynyl groups to high lying filled orbitals [41]. The differences might arise from the dissimilar type of calculation as well as from the fact that the two diimine ligand systems regarded (phen vs. ^{i}Pr–DAB) are not alike. In our calculations the first orbital with predominant metal character is $19a_1$, at 0.71 eV (5800 cm^{-1}) below the HOMO. The LUMO is mainly composed of the π*(^{i}Pr–DAB) orbital, with small platinum and C≡CH contributions. All in all, the electronic structure of [Pt(C≡CH)$_2$(^{i}Pr–DAB)] is very similar to that of [Pt(C≡CH)$_2$(COD)].

3.3.2. Spectroscopy and electronic transitions

Due to the lower energy of the LUMO, the ^{i}Pr–DAB complexes are all brightly colored in the solid state and in solution. Absorption spectra show several maxima in the visible and UV region. In the UV region complexes with substituents that do not contain π electrons (R = CH_3, neop, neoSi, adme) show only one intense band around 230 nm. All other studied compounds (R = Ph, Mes, C≡C^{t}Bu, C≡CPh, Cl) show additional intense absorptions in the UV at lower energy. In the visible region of the spectrum the first group of compounds exhibits two separate broad absorption bands that show marked structuring when investigated in non-polar solvents (Fig. 8). In polar solvents the bands are more or less unstructured and shift to higher energy (negative solvatochromism). Again the second group exhibits more complex behavior which results in occurrence or several maxima and overlap of the two band systems. Such structured absorption bands of platinum(II) complexes in non-polar solvents have been observed and were ascribed to vibronic structure [45]. For [Pt(CH_3)$_2$(^{i}Pr–DAB)] spectral deconvolution as shown in Fig. 8 gave constant spacing of about 1390 cm^{-1} for the maxima of the lowest set of absorption bands, but for other maxima in this complex no equal spacing was

Table 9
Selected G98/B3LYP calculated lowest TD DFT singlet excitation energies (eV) for [Pt(Me)$_2$(^{i}Pr–DAB)] and experimental absorption maxima

State	Main character	G98/B3LYP		G98/B3LYP solvent (CH_2Cl_2)		λ_{max} in nm [a] (ε in M^{-1} cm^{-1})
		Transition energy (eV)	Oscillator strength	Transition energy in eV (nm)	Oscillator strength	
$^1B_1$	98% ($19a_1 \rightarrow 11b_1$)	1.65	0.0009	1.99 (625)	0.0016	543 (2470)
$^1B_2$	99% ($8a2 \rightarrow 11b_1$)	1.86	0.0	2.09 (595)	0.0	507 (2000)
$^1B_1$	98% ($18a_1 \rightarrow 11b_1$)	2.28	0.0001	2.46 (505)	0.0001	470 (1020)
$^1A_1$	94% ($10b_1 \rightarrow 11b_1$)	3.02	0.118	3.12 (398)	0.113	390 (3340)
$^1B_2$	86% ($7a_2 \rightarrow 11b_1$)	5.04	0.128	4.99 (249)	0.157	

[a] From absorption spectra in CH_2Cl_2, maxima and extinction coefficients were extracted from spectral deconvolution.

found. In the rR spectrum of this complex we found only one very strong band ν(CN), therefore, we would only expect one vibronic mode that couples to the electronic transition.

Another reasonable assignment of such structuring would be the presence of several different electronic transitions. In order to assign the absorption bands and to resolve the matter of the observed closely spaced absorption bands as being vibrational fine structure or due to different electronic transitions, TD DFT calculations were performed for [Pt(Me)$_2$(^{i}Pr–DAB)] and for [Pt(C≡CH)$_2$(Me–DAB)]. Table 9 shows the TD DFT calculated characters and energies of the lowest-lying electronic transitions for [Pt(Me)$_2$(^{i}Pr–DAB)] using the GAUSSIAN 98 program package. The three lowest-energy are all overlap forbidden MLCT transitions from the three highest occupied orbitals to the lowest π*(^{i}Pr–DAB) orbital. The calculated vacuum transition energies are much lower than those observed in solution. In order to estimate the shift of transition energies due to the solvent effect, the solvent was modeled in G98/B3LYP calculations by polarized continuum model (PCM) [50]. Even when including CH_2Cl_2 as a solvent in the calculations, the values are still off by 1500–3000 cm^{-1}. This can be explained by the fact that the absorption band are significantly solvatochromic. For example in pentane the absorption bands occur at 518, 559, and 606 nm, which is significantly red-shifted from the values of 470, 507, and 543 nm found in CH_2Cl_2. Hence a small error in the modeling of the solvent has a strong influence on the calculated absorption maxima. The overlap allowed MLCT transition is much less solvatochromic (found at 414 nm in pentane and 390 nm in CH_2Cl_2), and concurrently the calculated value (398 nm in CH_2Cl_2) is much closer. In any case, we can conclude from the calculated transition energies that the lowest absorption bands cannot be ascribed to a vibrational fine-structure superimposed on the first overlap allowed transition (calculated at 398 nm in CH_2Cl_2), which is also of MLCT character. Apart from this MLCT transition, the ligand ππ* IL transition is calculated at 249 nm. The oscillator strengths calculated for the lowest three electronic transitions are very low. All these transitions are electronically allowed, hence the low oscillator strength is only due to poor calculated orbital overlap. However, in the absorption spectrum, the molar extinction coefficients are between 1000 and 2500 m^{-1} cm^{-1}, which is in the range of moderately allowed charge transfer transitions. Hence under real conditions (at ambient temperature, in solution), the allowedness is clearly increased. Already the change from vacuum to CH_2Cl_2 changes the calculated oscillator strength of the lowest transition almost twofold. Furthermore, because of the localization of the HOMO on the Pt atom, the inclusion of spin-orbit effect can influence the calculated intensity of transitions. At this point it seems that the three low-energy absorption bands observed in the absorption spectrum are due to different electronic transitions rather than to a vibrational progression superimposed on a single electronic transition. Below we will see that the rR spectra obtained by irradiation into these different absorption bands confirm the conclusions from these calculations. Like for the afore discussed COD–platinum(II) complexes, within the calculated spectral range we cannot find transitions between mainly platinum centered orbitals (LF transitions). If they occur they must be higher in energy than 200 nm. This can be already deduced from Table 6 where only the LUMO+2 ($16b_2$) has appreciable contributions from platinum orbitals but lies nearly 3.6 eV higher in energy than the LUMO $11b_1$. However, we cannot rule out the involvement of low-lying excited states with decent LF character since our calculations are not suited for such assignment.

Table 10 reports the low-lying electronic transitions of [Pt(C≡CH)$_2$(^{i}Pr–DAB)] as calculated by TD DFT. The calculated lowest-energy transition is the $20a_1 \rightarrow 11b_1$ one, which can be characterized as a mixed π(C≡C)/d(Pt) → π*(^{i}Pr–DAB) transition (L′LCT). The oscillator strength is quite low (0.0032) with respect to the found extinction coefficient (3250 M^{-1} cm^{-1}). This seems to be a general feature of TD DFT calculations for such complexes, since it was also found for the [Pt(R)$_2$(COD)] and [Pt(R)$_2$(^{i}Pr–DAB)] (R = Me, ^{i}Pr) complexes (see

Table 10
Selected calculated lowest TD DFT singlet excitation energies (eV and nm) for [Pt(C≡CH)$_2$(^{i}Pr–DAB)] together with experimentally observed values for [Pt(C≡C^{t}Bu)$_2$(^{i}Pr–DAB)]

State	Main character	G98/B3LYP		G98/B3LYP solvent (CH_2Cl_2)		λ_{max} in nm [a] (ε in M^{-1} cm^{-1})
		Transition energy (eV)	Oscillator strength	Transition energy in eV	Oscillator strength	
$^1B_1$	98% ($20a_1 \rightarrow 11b_1$)	1.58	0.0020	1.95 (638)	0.0032	477 (3.25)
$^1B_2$	99% ($8a_2 \rightarrow 11b_1$)	1.91	0.0001	2.19 (566)	0.0002	438 (0.88)
$^1B_1$	98% ($19a_1 \rightarrow 11b_1$)	2.63	0.0002	2.89 (428)	0.0003	410 (0.75)
$^1A_1$	94% ($10b_1 \rightarrow 11b_1$	3.18	0.095	3.29 (376)	0.092	393 (3.24)
$^1B_2$	86% ($20a_1 \rightarrow 17b_2$)	4.65	0.079	4.94 (253)	0.036	
$^1A_1$	94% ($8a_2 \rightarrow 9a_2$)	5.02	0.187	4.92 (252)	0.144	

[a] From absorption spectra in CH_2Cl_2, maxima and extinction coefficients were extracted from spectral deconvolution.

above). The calculated transition energy is much too low, even when including solvent modeling by PCM [50]. Thus, the lowest-energy absorption band is found in CH_2Cl_2 at 477 nm, while it is calculated at 638 nm (a difference of 5300 cm^{-1}). At higher energies more transitions from high-lying filled orbitals to the LUMO are calculated. They follow the same pattern of low oscillator strengths compared with the extinction coefficient and much too low transition energies. This makes unambiguous assignment to observed absorption bands difficult. However, it is presumed that although the calculated transition energies are wrong, the relative order of the transition does not change. The assignments reported in Table 10 are based on this assumption. Also for the other transitions the target orbital for the lowest electronic transitions is the LUMO in each case. The lowest transitions occur from orbitals that have mixed Pt(d)/C≡CR or nearly pure C≡CR character and we assign the long-wavelength absorptions, therefore, to mixed MLCT/L′LCT or L′LCT transitions (L′LCT = ligand (C≡CR)-to-ligand ($\pi^*_{diimine}$) charge transfer transitions. On first sight this contrasts to the MLCT assignment of the lowest excited states of diimine platinum(II) complexes with acetylide ligands [40–43]. However, our results from calculations and rR spectroscopy (see below) primarily focus on the lowest electronic transitions which might of course be different from the lowest excited states.

In order to get experimental information on the electronic transitions that belong to the low-energy absorption bands, rR spectra were recorded of the [Pt(R)$_2$(R′–DAB)] (R = CH_3, CD_3, C≡C^{t}Bu; R′ = ^{i}Pr, cHx) complexes dispersed in KNO_3. As mentioned in the introduction the rR spectrum shows which vibrations are influenced by the electronic transition that is excited. There are several instances in which rR was used to distinguish several electronic transitions within an apparently single absorption band [71,72]. Fig. 9 shows the rR spectra for [Pt(CH_3)$_2$(cHx–DAB)] for different excitation wavelengths, corresponding to the lowest-

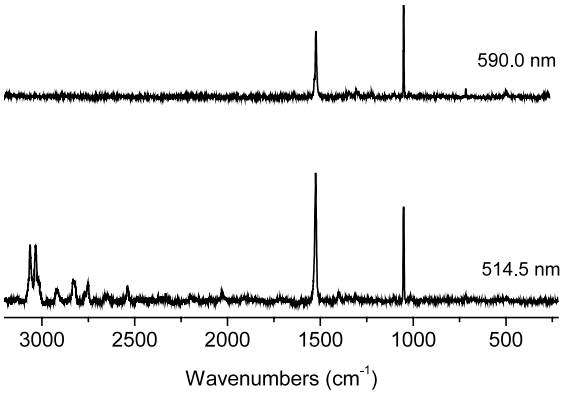

Fig. 9. rR spectra of [Pt(Me)$_2$(cHx–DAB)] in KNO_3, recorded with two different excitation wavelengths.

energy two components of the first set of absorption bands. Clearly, the spectra are different depending on the excitation wavelength, which supports the assignment of these absorption bands to different electronic transitions. For the complex [Pt(C≡C^{t}Bu)$_2$(^{i}Pr–DAB)] irradiation into the long-wavelength transition leads to a strong enhancement of a band at 2132 cm^{-1} that we assign to the C≡C stretching mode ν(CC). This enhancement strongly supports the contribution of orbitals from the C≡C^{t}Bu ligand to the HOMOs and the L′LCT or mixed MLCT/L′LCT character of these transitions. Using time-resolved FTIR spectroscopy Schanze et al. have found that the frequency of the ν(CC) mode in complexes [Pt(C≡CR)$_2$(R′–bpy)] (R = Aryl, R′–bpy = alkyl substituted bpy) are about 25–35 cm^{-1} higher in the excited states of the molecules than in their ground states which served as indication for an MLCT character of the excited state [42]. However, their investigations focus on the thermally relaxed excited state whereas rR provides direct information on the electronic transition. That these can be very different was recently shown by comparison of these two techniques [73]. From the striking agreement of our

calculations and rR results we conclude that the C≡CR group is directly involved in the electronic transition. A full investigation of the rR spectra will be published elsewhere [46].

3.3.3. Photochemistry

In the above we showed that the visible absorption bands of the [Pt(R)$_2$(^{i}Pr–DAB)] complexes belong to electronic transitions with some contribution from R group orbitals. The involvement of these orbitals could give rise to observable photochemistry, like in the case of the [Pt(R)$_2$(COD)] compounds (see Section 2.1). Therefore, the photochemical reactivity of the complexes [Pt(R)$_2$(^{i}Pr–DAB)] (R = Me, neop, neoSi, adme, Ph, Mes, C≡C^{t}Bu, C≡CPh; see Section 2.1 for abbreviations) was investigated by broadband irradiation of solutions of the complexes into the set of the three lowest-lying absorption bands using suitable cut-off filters. Under these conditions, many of the complexes are indeed photoreactive in several common organic solvents such as THF, dichloromethane or acetonitrile. For the complexes with R = Ph, Mes, C≡C^{t}Bu, C≡CPh no photoreactivity was observed upon irradiation into their lowest set of three absorption bands. For the remaining complexes the relative reactivities (in 10^{-5} M oxygen free solutions in THF) were determined by observing the decay of the absorption band of the parent complex as a function of irradiation time. The results show that the photochemical reactivity increases in the order Me < neoSi < neop < adme, which is the same order as found for the COD complexes. Irradiation into the second absorption band at higher energy ($\lambda > 400$ nm) accelerates the photoreactions by a factor of 1.5–2. Irradiation at even higher energy (320 nm < $\lambda < 350$ nm) results in very efficient photodecomposition for the reactive compounds and measurable reactivity even for the alkynyl complexes.

In order to study the product formation, the photoreactions of the complexes dissolved in CD_2Cl_2 ($\sim 10^{-3}$ M) upon irradiation into their lowest absorption bands were followed by ^{1}H-NMR spectroscopy. Similarly to the COD complexes (Section 2.1) the main observed product is the monochlorinated complex [Pt(Cl)(R)(^{i}Pr–DAB)]. This suggests that the primary photochemical step is Pt–C bond homolysis, followed by chlorine abstraction from the solvent by the organometallic radical. In non-chlorinated solvents the photolysis products cannot be clearly defined. In most cases elemental platinum drops from the solutions, which points to a photochemically induced reductive elimination. However, the bialkyl products, which should remain in solution for the heavier alkyls, were not the only products observed. In addition, the free ligand was not observed, which can be due to its alkylation by the $^\bullet$R radicals. In the case of Zn(R)$_2$(R′–DAB) complexes, thermal and photochemical $^\bullet$R radical formation can lead to clean formation N- and C-alkylated DAB derivatives [67,74–76], but this is not the case for the present complexes, nor for the [Pt(Me)$_4$(^{i}Pr–DAB)] complexes (see below). For the alkynyl complexes, irradiation of solutions of these compounds at very high energy gives rise to a clear reaction sequence yielding exclusively elemental platinum, the free ligand and the coupled dialkynyls R′–C≡C–C≡C–R′ (R′ = ^{t}Bu or Ph), corresponding to a reductive elimination reaction similar to the photoreaction observed for the [Pt(C≡CR′)$_2$(COD)] complexes (Section 2.1).

In order to study the wavelength dependence of the photoreactivity of the [Pt(R)$_2$(^{i}Pr–DAB)] complexes in more detail, the complex with R = neop was chosen as one of the most reactive samples. Irradiation of an oxygen free dichloromethane solution of [Pt(neop)$_2$(^{i}Pr–DAB)] into its lowest-energy absorption band (at 590 nm in this solvent) by using a high pressure Xe lamp fitted with a $\lambda > 600$ nm cut-off filter did not result in observable photoreactivity. Irradiation into the second absorption band (at 556 nm), using a 552 dye laser (Coumarin 6) line, did however, (Fig. 10). On irradiation using intense Ar^+ laser light ($\lambda = 514.5$ nm, power ~ 10 mW) we measured a photochemical quantum yield of 0.000726 for the photochemical reaction. For the complexes [Pt(R)$_2$(COD)] a decrease of a factor of 42 was observed going from R = neop to Me (Section 2.1). Since a photochemical quantum yield of 0.005 was found for the oxidative addition of MeI to [Pt(Me)$_2$(COD)] [65], it is obvious that substitution of the COD ligand by ^{i}Pr–DAB leads to a dramatic decrease in photoreactivity. This correlates well to the finding from the theoretical calculations where the contribution of the R groups to the HOMO decreases on going from COD to ^{i}Pr–DAB e.g. for the R = CH$_3$ system from 31 to 12%.

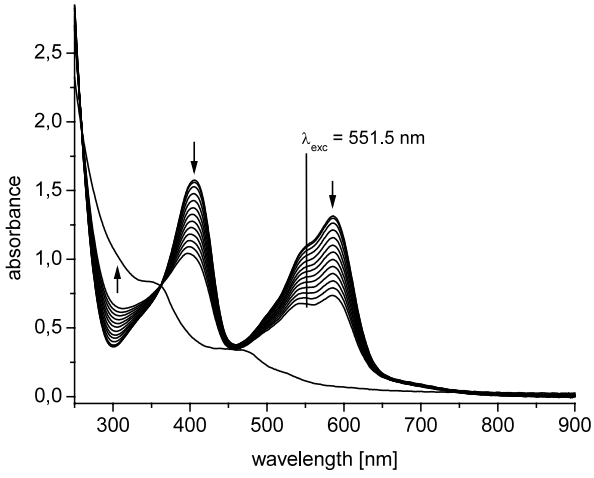

Fig. 10. Absorption spectra of [Pt(neop)$_2$(^{i}Pr–DAB)] in CH_2Cl_2, during photolysis ($\lambda_{ex} = 552$ nm). The last spectrum represents [Pt(Cl)(neop)(^{i}Pr–DAB)].

In the next section we move to platinum(IV) complexes [Pt(Me)$_4$(^{i}Pr–DAB)]. It will be shown that these complexes are much more photoreactive, due to the fact that their electronic structures are different.

4. Metal–carbon bonded platinum(IV) complexes

4.1. Introduction

This section describes the electronic structure, electronic transitions and the photochemistry of a class of platinum(IV) complexes, [Pt(Me)$_4$(R–DAB)] (R–DAB = *N*,*N*′-diorgano-1,4-diazabutadiene). A number of photochemical studies of platinum(IV) complexes are known [57]. Irradiation of solutions of the platinum(IV) metallacyclobutane complexes [Pt(X)$_2$($CH_2CH_2CH_2$)-(L$_2$)] (X = Cl, Br; L$_2$ = phen, bpy, tetramethylethylenediamine, 2-MeCN, 2-py) gave rise to propene formation in relatively non-polar solvents via reductive elimination and to cyclopropane formation in polar ones. This latter product is formed in a thermal way after halide dissociation from the excited state. The nature of the electronic transitions and excited states was not investigated. Under the same conditions the [Pt(I)$_2$($CH_2CH_2CH_2CH_2$)(L$_2$)] (L = PMe_2Ph, PPh_3) complexes yielded ethylene and 1-butene as photolysis products. Photochemical Pt–CH_3 bond homolysis was observed on irradiation of [Pt(Cp)(Me)$_3$] as demonstrated by EPR spectroscopy. The photolysis [Pt(I)(Me)(Ph)$_2$(bpy)] and [Pt(I)(Me)$_3$(bpy)] gave rise to several organic photoproducts. The formation of these products was suggested to involve Pt–CH_3 and Pt–Ph photochemical bond homolysis as the primary photochemical step. The lowest-energy electronic transition was shown to have XLCT (X = I) character in the case of [Pt(I)(Me)$_3$(α-diimine)] complexes by DFT calculations and rR spectroscopy [28]. Finally, it was noted that [Pt(Me)$_4$(bpy)]′ appears to be photosensitive and a chloroform solution decomposed to [Pt(Cl)(Me)$_3$(bpy)] on standing. This qualitative remark was followed by more detailed work from the groups of Puddephatt [77,78], and Kaim [26,79]. The results from these studies as well as our own are discussed below. As above, first the electronic structure and transitions are considered, which is followed by a discussion of the photochemical properties.

4.2. [Pt(Me)$_4$(α-diimine)] complexes

4.2.1. Electronic structure

From investigations of the thermal reactions of [Pt(Me)$_4$(α-diimine)] (α-diimine = bpy, phen) complexes, it was concluded that the HOMO of these complexes has σ(Pt–CH_3) character, where the CH_3 is one of the mutually *trans* located ones [80]. This was later confirmed by hybrid density functional theory/Hartree–Fock (DFT/HF) calculations on the [Pt(Me)$_4$(H–DAB)] model system [26]. These calculations showed that the HOMO consists of the antisymmetric combination of the sp^3 hybrid orbitals of the axial methyl groups, with the addition of a small p(Pt) contribution. The LUMO is mainly located on the π*(H–DAB) ligand. These calculations were later repeated on the real [Pt(Me)$_4$(^{i}Pr–DAB)] molecule [28]. The results of these calculations are shown in Table 11. The 13b$_1$ HOMO (Fig. 11) is indeed mainly composed of the axial methyl groups, with a small Pt contribution. Hence it is best described as a σ(C_{ax}–Pt–C_{ax}) orbital. The 14b$_1$ LUMO (Fig. 12) has predominant π*(^{i}Pr–DAB) character. Some delocalization of the σ and π* orbitals occurs. Thus, the HOMO has 13% π*(^{i}Pr–DAB) character, while the axial methyl groups contribute 14% to the LUMO. This mixing was found to an even higher degree for other d^6 transition metal–diimine model complexes with two σ donating axial ligands. For instance the model complex [Ru(SnH_3)$_2$(CO)$_2$(H–DAB)] [81] has 27% H–DAB contribution to the HOMO and the same percentage of the axial SnH_3 groups to the LUMO. The platinum(IV) model complex [Pt(SnH_3)$_2$(Me)$_2$(^{i}Pr–DAB)] has slightly less σ–π* mixing at 18% ^{i}Pr–DAB contribution to the HOMO and 23% SnH_3 to the LUMO [28]. The metal–methyl complex [Ru(Me)(SnH_3)(H–DAB)] has about the same degree of mixing of σ and π* orbitals as the corresponding bis-SnH_3 compound [23]. It is clear that the results for [Pt(Me)$_4$(^{i}Pr–DAB)] agree with the previous calculations on the H–DAB model complex and, therefore, the simplification of the α-diimine ligand is of minor influence on the electronic structure of the complexes. Since the HOMO and LUMO are of the same symmetry, the HOMO → LUMO transition is strongly overlap allowed, which is also clear from the observed σ–π* mixing. The following section describes the electronic transitions of [Pt(Me)$_4$(^{i}Pr–DAB)] as studied by experimental and theoretical methods.

4.2.2. Spectroscopy and electronic transitions

All the [Pt(Me)$_4$(α-diimine)] complexes are strongly colored in the solid state and in solutions (Fig. 13), in contrast to most alkyl–platinum(IV) complexes, which are usually colorless, or pale yellow. For example the lowest-energy absorption band of [Pt(I)(Me)$_3$(^{i}Pr–DAB)] lies at 432 nm in toluene, while that of [Pt(Me)$_4$(^{i}Pr–DAB] was observed at 531 nm in the same solvent [28]. That observation together with the assignment of the HOMO and LUMO orbitals, led to the assignment of the visible absorption band to a σ(Pt–C) → π(α-diimine) transition [26,77–79]. Since such an electronic transition removes electron density from the σ(Pt–C) orbital, the photolability of the complexes agrees with the proposed assignment. In the following

Table 11
DFT calculated one-electron energies and percentage composition of selected highest-occupied and lowest-unoccupied molecular orbitals of [Pt(Me)$_4$(^{i}Pr–DAB)] expressed in terms of composing fragments

MO	E (eV)	Prevailing character	Pt	(Me)$_{ax}$	(Me)$_{eq}$	^{i}Pr–DAB
Unoccupied						
17b$_2$	−0.20	d$_{Pt}$+Me+^{i}Pr–DAB	2 (p$_y$); 33 (d$_{yz}$)		48	16
10a$_2$	−0.39	π* R–DAB	1 (d$_{xy}$)			99
14b$_1$	−3.35	π* R–DAB+(Me)$_{ax}$	8 (d$_{xz}$); 1 (p$_x$)	14		77 (π*)
Occupied						
13b$_1$	−4.79	Me$_{ax}$+Pt+π* R–DAB	9 (p$_x$); 1 (d$_{xz}$)	73	3	13
9a$_2$	−5.48	d$_{Pt}$+π* R–DAB	75 (d$_{xy}$)	8	4	12
21a$_1$	−5.71	d$_{Pt}$+Me$_{eq}$	53 (d$_{z^2}$); 20 (d$_{x^2-y^2}$)		17	7
12b$_1$	−5.93	d$_{Pt}$+R–DAB	71 (d$_{xz}$); 1 (p$_x$)	10	6	12

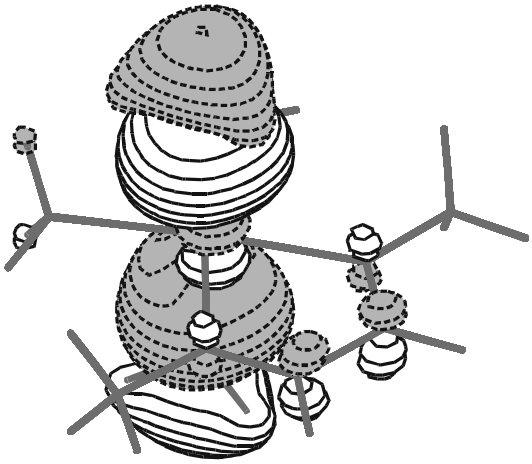

Fig. 11. 13b$_1$ HOMO [Pt(Me)$_4$(^{i}Pr–DAB)].

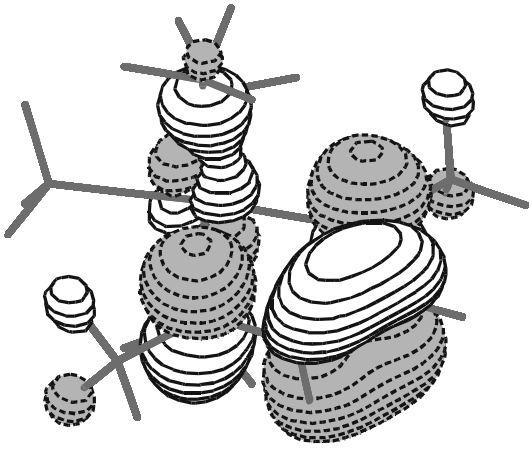

Fig. 12. 14b$_1$ LUMO [Pt(Me)$_4$(^{i}Pr–DAB)].

two more pieces of evidence are discussed which support this assignment, namely TD DFT calculations and rR spectra.

Table 12 shows the results of the TD DFT calculations of low-lying electronic transitions. Indeed the lowest-energy one has 93% 13b$_1$→14b$_1$ character which corresponds to the HOMO→LUMO or σ(Me–Pt–

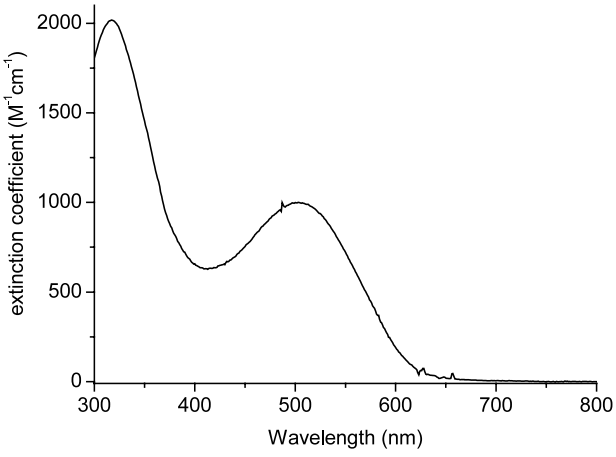

Fig. 13. Absorption spectrum of [Pt(Me)$_4$(^{i}Pr–DAB)] in THF at room temperature.

Me)→π*(^{i}Pr–DAB) SBLCT transition. At higher energy an overlap forbidden MLCT transition is calculated which is not observed in the spectrum, in agreement with its low calculated oscillator strength. The next transition has MLCT character as well, but since this transition is overlap allowed, it gives rise to a strong absorption band in the spectrum. The calculated transition energies of the two allowed transitions (623 and 386 nm) are much lower than the observed ones (531 and 326 nm). This difference is probably due to the difference in medium between calculation and experiment. All calculations were performed in vacuum, while the absorption maximum values are determined in toluene. Since the absorption bands are quite solvatochromic ($\Delta\nu = \nu(\text{MeCN}) - \nu(\text{toluene}) = 2044\ \text{cm}^{-1}$), such a difference in medium can lead to appreciable differences in transition energy. This was noted before in the case of the [Pt(Me)$_2$(^{i}Pr–DAB)] complex (Section 3.3), where inclusion of the solvent in the calculations led to enormously improved values for the transition energies.

The assignment of the lowest-energy electronic transition was further supported by rR spectra recorded upon irradiation into that absorption band. Fig. 14 shows the

Table 12
TD DFT calculated lowest-energy singlet excitation energies and observed absorption maxima of [Pt(Me)$_4$(^{i}Pr–DAB)]

State	Composition	Calculated transition energy		λ_{abs} (nm) [a]	Calculated oscillator strength
		(eV)	(nm)		
$^1A_1$	93% ($13b_1 \rightarrow 14b_1$)	1.99	623	531	0.021
$^1B_2$	94% ($9a_2 \rightarrow 14b_1$)	2.26	549	n.o. [b]	0.002
$^1A_1$	91% ($12b_1 \rightarrow 14b_1$)	3.21	386	326	0.072

[a] Observed wavelength maximum in toluene at room temperature.
[b] Not observed.

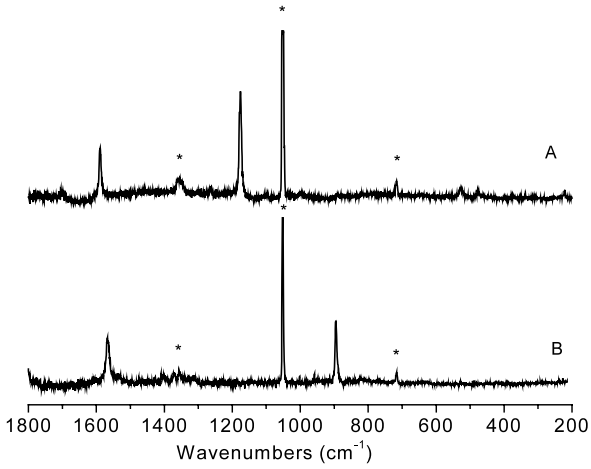

Fig. 14. rR spectra of [Pt(CH$_3$)$_4$(^{i}Pr–DAB)] (A) and [Pt(CD$_3$)$_4$(^{i}Pr–DAB)] (B) in KNO_3, recorded on irradiation into the lowest-energy absorption band.

rR spectra of [Pt(CH$_3$)$_4$(^{i}Pr–DAB)] and its deuterated derivative [Pt(CD$_3$)$_4$(^{i}Pr–DAB)]. In order to assign all the observed rR bands unambiguously, vibrational calculations were performed using DFT methods. The band observed at 1564 and 1567 cm^{-1} for the CH$_3$ and CD$_3$ complexes respectively is assigned to the symmetrical CN stretch, ν_s(CN), in agreement with the calculated values of 1592 and 1585 cm^{-1}, respectively. The values are about 2% too high, which is quite normal for calculations of this level. As noted in the introduction (Section 1), in general in rR spectra only those vibrations are observed which are influenced by the electronic transition which is excited. Therefore, the observation of ν_s(CN) in the rR spectrum is in accordance with the fact that the charge which is transferred during the electronic transition end up in the π* orbital of the ^{i}Pr–DAB ligand, since this orbital is antibonding with respect to the CN bond. Much more unusual is the observation of a band at 1175 cm^{-1} for the CH$_3$ complex and at 894 cm^{-1} CD$_3$ complex. In line with the calculated values of 1221 and 931 cm^{-1} and the observed deuteration effect, these bands are ascribed to an umbrella-like movement of the axial methyl groups, δ_s(CH$_3$)/(CD$_3$) [28]. This vibration was not observed as a strong band for [Pt(I)(Me)$_3$(^{i}Pr–DAB)] or the structurally and electronically similar [Ru(X)(Me)(CO)$_2$(^{i}Pr–DAB)] complexes [5,27,28]. It gives a clear indication of the involvement of the axial methyl groups in the electronic transition and strongly supports its assignment to an SBLCT transition, since removal of electron density from the axial ligands will influence the bonds and angles of the methyl groups. Interestingly, the first overtone of the δ_s(CH$_3$)/(CD$_3$) is observed as well as the combination band of this band with the one due to ν_s(CN). The symmetrical C$_{ax}$–Pt–C$_{ax}$ stretching vibration is also affected by the SBLCT transition and observed as a weak band at about 470 cm^{-1} (calculated 574 cm^{-1}). The band at ca. 520 cm^{-1} is ascribed to the symmetrical C$_{eq}$–Pt–C$_{eq}$ stretching vibration on the basis of the calculations (calculated 497 cm^{-1}).

Since the lowest electronic transition of the [Pt(Me)$_4$(α-diimine)] complexes has SBLCT character, the observed photolability of the complexes is not surprising. The following section treats this subject in some more detail.

4.2.3. Photochemistry

Excitation to the ^{1}SBLCT state is expected to lead to rapid intersystem crossing (ISC) to the corresponding ^{3}SBLCT state. Indeed the excited state could be quenched by the triplet quencher perylene. From the quencher concentration dependence an excited state lifetime of $\sim 10^{-8}$ s was estimated for [Pt(Me)$_4$(bpy)] [77]. The σ(C$_{ax}$–Pt–C$_{ax}$) → π*(α-diimine) transition removes electron density from the σ(C$_{ax}$–Pt–C$_{ax}$) bond. This bond is already weak in the ground state, e.g. the crystal structure of [Pt(Me)$_4$(cHx–DAB)] shows that the Pt–C$_{ax}$ bond length is significantly longer (2.140(8) Å) than the Pt–C$_{eq}$ one (2.045(5) Å) [45]. Therefore, it is not surprising that the primary photochemical step is Pt–C$_{ax}$ bond homolysis. The $^\bullet$Me radical resulting from irradiation of solutions of [Pt(Me)$_4$(^{i}Pr–DAB)] was directly observed by time-resolved FT-EPR spectroscopy, and identified by the hyperfine coupling constants (hfcc) of the odd electron to the ^{1}H nuclear spins [82]. These experiments confirmed the triplet character of the excited state. The metal fragment radical is not observed under these conditions. However, irradiation of a diethyl ether solution of [Pt(Me)$_4$(^{t}Bu–DAB)] at 240 K in the presence of the spin trap 2-methyl-2-

nitrosopropane (^{t}Bu–NO) gave rise to an EPR spectrum that was identified as the spin-trapped metal fragment by the observed g value of 2.0060 and the 4.0 mT ^{195}Pt hfcc [79]. The methyl radical was trapped in experiments in dichloromethane or benzene in the presence of 5,5-dimethylpyrroline-*N*-oxide (dmpo) and identified by the ^{1}H hfcc [78].

Both radical species are obviously very reactive. Some effort has been made to analyze the products obtained from photolysis experiments. In chlorinated solvents the 17e$^-$ [Pt(Me)$_3$(α-diimine)]$^\bullet$ radical efficiently abstracts a chlorine atom from the solvent resulting in [Pt(Cl)(Me)$_3$(α-diimine)] [26,78]. In non-chlorinated solvents the presence of several oligomethyl platinum species were observed in the ^{1}H- or ^{13}C-NMR spectra upon irradiation into the SBLCT band of [Pt(Me)$_4$(R–DAB)] (R = ^{t}Bu, *p*Tol). Irradiation at higher energies led to formation of platinum metal and some methane [26]. All these photochemical reactions occur with great efficiency, with quantum yields for the photoreaction of [Pt(Me)$_4$(bpy)] ranging from 0.8 to unity in various solvents.

From CIDNP experiments, more intricate information about the mechanism of the photoreactions of [Pt(Me)$_4$(bpy)] in $CDCl_3$ was obtained [78], showing that the initially formed methyl radical can react with another methyl radical to give ethane. Furthermore, it can react with a solvent molecule forming monodeuterated methane. The $^\bullet CCl_3$ radical that is thus formed, can react with another methyl radical resulting in CH_3CCl_3. Alternatively, the platinum radical can abstract a chlorine atom from the solvent, after which the resulting $^\bullet CDCl_2$ radical can react with a methyl radical, yielding CH_3CDCl_2. Interestingly, irradiation of [Pt(Me)$_4$(bpy)] in the presence of all sorts of organic molecules, e.g. carboxylic esters, terminal acetylenes, gave rise to carboxylate and acetylide derivatives of the photochemically formed platinum radical [77].

Due to the reactivity of the R–DAB ligand, this ligand can be alkylated by the methyl radical. Bulk photolysis of [Pt(Me)$_4$(R–DAB)] and subsequent work up, including hydrolysis, showed the presence of several amino aldehyde products which are derived from such methylated R–DAB compounds. As mentioned before, similar thermal and photochemical alkylations of R–DAB ligands are known in the case of the main group [Zn(R)$_2$(R–DAB)] compounds [67,74–76]. However, in the latter case, depending on conditions, these reactions can lead to very cleanly C- or N-alkylated R–DAB derivatives.

Acknowledgements

This work was carried out in the framework of the COST D14 action. Axel Klein would like to thank Professor D.J. Stufkens (University of Amsterdam) for the opportunity to do research in his group and also for fruitful discussions and Professor W. Kaim is acknowledged for financial support. Stanislav Záliš thanks also for the financial support from the Ministry of Education of the Czech Republic (OC.D14.20).

References

[1] V. Balzani, A. Juris, Coord. Chem. Rev. 211 (2001) 97.
[2] A. Hagfeldt, M. Grätzel, Acc. Chem. Res. 33 (2000) 269.
[3] C.A. Bignozzi, R. Argazzi, C.J. Kleverlaan, Chem. Soc. Rev. 29 (2000) 87.
[4] F. Barigelletti, L. Flamigni, Chem. Soc. Rev. 29 (2000) 1.
[5] H.A. Nieuwenhuis, D.J. Stufkens, A. Oskam, Inorg. Chem. 33 (1994) 3212.
[6] B.D. Rossenaar, D.J. Stufkens, A. Vlček, Jr., Inorg. Chem. 35 (1996) 2902.
[7] R.J.H. Clark, T.J. Dines, Angew. Chem. Int. Ed. Engl. 25 (1986) 131.
[8] M. Turki, C. Daniel, S. Záliš, A. Vlček, Jr., J. van Slageren, D.J. Stufkens, J. Am. Chem. Soc. 123 (2001) 11431.
[9] H.A. Nieuwenhuis, D.J. Stufkens, A. Vlček, Jr., Inorg. Chem. 34 (1995) 3879.
[10] D.J. Stufkens, A. Vlček, Jr., Coord. Chem. Rev. 177 (1998) 127.
[11] K.S. Schanze, D.B. MacQueen, T.A. Perkins, L.A. Cabana, Coord. Chem. Rev. (1993) 63.
[12] R.J. Shaver, M.W. Perkovic, D.P. Rillema, C. Woods, Inorg. Chem. 34 (1995) 5446.
[13] L.A. Lucia, Y. Wang, K. Nafisi, T.L. Netzel, K.S. Schanze, J. Phys. Chem. 99 (1995) 11801.
[14] P.I. Djurovich, R.J. Watts, Inorg. Chem. 32 (1993) 4681.
[15] J.C. Luong, R.A. Faltynek, M.S. Wrighton, J. Am. Chem. Soc. 101 (1979) 1597.
[16] C.J. Kleverlaan, D.J. Stufkens, I.P. Clark, M.W. George, J.J. Turner, D.M. Martino, H. van Willigen, A. Vlček, Jr., J. Am. Chem. Soc. 120 (1998) 10871.
[17] I.R. Farrell, P. Matousek, C.J. Kleverlaan, A. Vlček, Jr., Chem. Eur. J. 6 (2000) 1386.
[18] B.D. Rossenaar, C.J. Kleverlaan, M.C.E. van de Ven, D.J. Stufkens, A. Vlček, Jr., Chem. Eur. J. 2 (1996) 228.
[19] H.A. Nieuwenhuis, M.C.E. van de Ven, D.J. Stufkens, A. Oskam, K. Goubitz, Organometallics 14 (1995) 780.
[20] J. van Slageren, A.L. Vermeer, D.J. Stufkens, M. Lutz, A.L. Spek, J. Organomet. Chem. 626 (2001) 118.
[21] J. van Slageren, D.J. Stufkens, Inorg. Chem. 40 (2001) 277.
[22] J. van Slageren, F. Hartl, D.J. Stufkens, Eur. J. Inorg. Chem. (2000) 847.
[23] M.P. Aarnts, D.J. Stufkens, M.P. Wilms, E.J. Baerends, A. Vlček, Jr., I.P. Clark, M.W. George, J.J. Turner, Chem. Eur. J. 2 (1996) 1556.
[24] J.C. Luong, R.A. Faltynek, M.S. Wrighton, J. Am. Chem. Soc. 102 (1980) 7892.
[25] B.D. Rossenaar, E. Lindsay, D.J. Stufkens, A. Vlček, Jr., Inorg. Chim. Acta 250 (1996) 5.
[26] W. Kaim, A. Klein, S. Hasenzahl, H. Stoll, S. Záliš, J. Fiedler, J. Organomet. 17 (1998) 237.
[27] J. van Slageren, A. Klein, S. Záliš, D.J. Stufkens, Coord. Chem. Rev. 219-221 (2001) 937.
[28] J. van Slageren, D.J. Stufkens, S. Záliš, A. Klein, J. Chem. Soc. Dalton Trans. (2002) 218.
[29] A. Vogler, H. Kunkely, Comments Inorg. Chem. 9 (1990) 201.
[30] W. Paw, S.D. Cummings, M.A. Mansour, W.B. Connick, D.K. Geiger, R. Eisenberg, Coord. Chem. Rev. 171 (1998) 125.

[31] S.D. Cummings, R. Eisenberg, J. Am. Chem. Soc. 118 (1996) 1949.
[32] J.A. Weinstein, N.N. Zheligovskaya, M.Y. Mel'nikov, F. Hartl, J. Chem. Soc. Dalton Trans. (1998) 2459.
[33] T.M. Cocker, R.E. Bachman, Inorg. Chem. 40 (2001) 1550.
[34] R. Benedix, H. Hennig, Inorg. Chim. Acta 141 (1988) 21.
[35] W.B. Connick, D. Geiger, R. Eisenberg, Inorg. Chem. 38 (1999) 3264.
[36] J. Biedermann, G. Gliemann, U. Klement, K.-J. Range, M. Zabel, Inorg. Chem. 29 (1990) 1884.
[37] J. Biedermann, G. Gliemann, U. Klement, K.-J. Range, M. Zabel, Inorg. Chim. Acta 169 (1990) 63.
[38] V.H. Houlding, V.M. Miskowski, Coord. Chem. Rev. 111 (1991) 145.
[39] K.E. Dungey, B.D. Thompson, N.A.P. Kane-Maguire, L.L. Wright, Inorg. Chem. 39 (2000) 5192.
[40] M. Hissler, J.E. McGarrah, W.B. Connick, D.K. Geiger, S.D. Cummings, R. Eisenberg, Coord. Chem. Rev. 208 (2000) 115.
[41] M. Hissler, W.B. Connick, D.K. Geiger, J.E. McGarrah, D. Lipa, R.J. Lachicotte, R. Eisenberg, Inorg. Chem. 39 (2000) 447.
[42] C.E. Whittle, J.A. Weinstein, M.W. George, K.S. Schanze, Inorg. Chem. 40 (2001) 4053.
[43] C.-M. Che, L.-Y. He, C.-K. Poon, T.C. Mak, Inorg. Chem. 28 (1989) 3081.
[44] A. Klein, J. van Slageren, S. Záliš, J. Organomet. Chem. 620 (2001) 202.
[45] S. Hasenzahl, H.-D. Hausen, W. Kaim, Chem. Eur. J. 1 (1995) 95.
[46] A. Klein, J. van Slageren, S. Záliš, Inorg. Chem. submitted.
[47] C. Fonseca Guerra, J.G. Snijders, G. te Velde, E.J. Baerends, Theor. Chim. Acc. 99 (1998) 391.
[48] S.J.A. van Gisbergen, J.G. Snijders, E.J. Baerends, Comput. Phys. Commun. 118 (1999) 119.
[49] M.J. Frisch, G.W. Trucks, H.B. Schlegel, G.E. Scuseria, M.A. Robb, J.R. Cheeseman, V.G. Zakrzewski, J.J.A. Montgomery, R.E. Stratmann, J.C. Burant, S. Dapprich, J.M. Millam, A.D. Daniels, K.N. Kudin, M.C. Strain, O. Farkas, J. Tomasi, V. Barone, M. Cossi, R. Cammi, B. Mennucci, C. Pomelli, C. Adamo, S. Clifford, J. Ochterski, G.A. Petersson, P.Y. Ayala, Q. Cui, K. Morokuma, D.K. Malick, A.D. Rabuck, K. Raghavachari, J.B. Foresman, J. Cioslowski, J.V. Ortiz, B.B. Stefanov, G. Liu, A. Liashenko, P. Piskorz, I. Komaromi, R. Gomperts, R.L. Martin, D.J. Fox, T. Keith, M.A. Al-Laham, C.Y. Peng, A. Nanayakkara, C. Gonzalez, M. Challacombe, P.M.W. Gill, B. Johnson, W. Chen, M.W. Wong, J.L. Andres, C. Gonzalez, M. Head-Gordon, E.S. Replogle, J.A. Pople, Gaussian 98, Inc., Pittsburgh PA, 1998.
[50] C. Amovilli, V. Barone, R. Cammi, E. Cances, M. Cossi, B. Mennucci, C.S. Pomelli, J. Tomasi, Adv. Quantum Chem. 32 (1999) 227.
[51] A.D. Becke, Phys. Rev. A 38 (1988) 3098.
[52] J.P. Perdew, Phys. Rev. A 33 (1986) 8822.
[53] E. van Lenthe, A. Ehlers, E.J. Baerends, J. Chem. Phys. 110 (1999) 8943.
[54] D.E. Woon, T.H. Dunning, Jr., J. Chem. Phys. 98 (1993) 1358.
[55] D. Andrae, U. Häussermann, M. Dolg, H. Stoll, H. Preuss, Theor. Chim. Acta 77 (1990) 123.
[56] P.J. Stephens, F.J. Devlin, C.F. Cabalowski, M.J. Frisch, J. Phys. Chem. 98 (1994) 11623.
[57] D.B. Pourreau, G.L. Geoffroy, Adv. Organomet. Chem. 24 (1985) 249 (and references therein).
[58] D.C.L. Perkins, R.J. Puddephatt, C.F.H. Tipper, J. Organomet. Chem. 191 (1980) 481.
[59] P.W.N.M. van Leeuwen, C.F. Roobeek, R. Huis, J. Organomet. Chem. 142 (1977) 243.
[60] A. Hudson, M.F. Lappert, P.W. Lednor, J.J. MacQuitty, B.K. Nicholson, J. Chem. Soc. Dalton Trans. (1981) 2159.
[61] J. Müller, P. Göser, Angew. Chem. Int. Ed. Engl. 6 (1967) 364.
[62] L.L. Constanzo, S. Giuffrida, R. Romeo, Inorg. Chem. 20 (1980) 789.
[63] R.H. Hill, R.J. Puddephatt, J. Am. Chem. Soc. 107 (1985) 1218.
[64] J.A.M van Beek, G. van Koten, I.C.M. Wehmann-Ooyevaar, W.J.J. Smeets, P. van der Sluis, A.L. Spek, J. Chem. Soc. Dalton Trans. (1991) 883.
[65] H. Kunkely, A. Vogler, J. Organomet. Chem. 553 (1998) 517.
[66] D.A. Roberts, W.R. Mason, G.L. Geoffroy, Inorg. Chem. 20 (1981) 789.
[67] M. Kaupp, H. Stoll, H. Preuss, W. Kaim, T. Stahl, G. van Koten, E. Wissing, W.J.J. Smeets, A.L. Spek, J. Am. Chem. Soc. 113 (1991) 5606.
[68] P.S. Braterman, Top. Curr. Chem. 92 (1980) 149.
[69] W.B. Connick, H.B. Gray, J. Am. Chem. Soc. 117 (1997) 11620.
[70] Y. Zhang, K.D. Ley, K.S. Schanze, Inorg. Chem. 35 (1996) 7102.
[71] R.W. Balk, D.J. Stufkens, A. Oskam, Inorg. Chim. Acta 34 (1979) 267.
[72] K.-S.K. Shin, J.I. Zink, J. Am. Chem. Soc. 112 (1990) 7148.
[73] J.A. Weinstein, J. van Slageren, D.J. Stufkens, S. Zalis, M.W. George, J. Chem. Soc. Dalton Trans. (2001) 2587.
[74] J.M. Klerks, J.T.B.H. Jastrzebski, G. van Koten, K. Vrieze, J. Organomet. Chem. 224 (1982) 107.
[75] G. van Koten, J.T.B.H. Jastrzebski, J. Organomet. Chem. 250 (1983) 49.
[76] E. Rijnberg, J. Boersma, J.T.B.H. Jastrzebski, M.T. Lakin, A.L. Spek, G. van Koten, Organometallics 16 (1997) 3158.
[77] J.E. Hux, R.J. Puddephatt, J. Organomet. Chem. 346 (1988) C31.
[78] J.E. Hux, R.J. Puddephatt, J. Organomet. Chem. 437 (1992) 251.
[79] A. Klein, S. Hasenzahl, W. Kaim, J. Chem. Soc. Perkin Trans. 2 (1997) 2573.
[80] J.E. Hux, R.J. Puddephatt, Inorg. Chim. Acta 100 (1985) 1.
[81] M.P. Aarnts, M.P. Wilms, K. Peelen, J. Fraanje, K. Goubitz, F. Hartl, D.J. Stufkens, E.J. Baerends, A. Vlček, Jr., Inorg. Chem. 35 (1996) 5468.
[82] J. van Slageren, D.M. Martino, C.J. Kleverlaan, A.P. Bussandri, H. van Willigen, D.J. Stufkens, J. Phys. Chem. A 104 (2000) 5969.